Environmental Science Nano

ROYAL SOCIETY OF CHEMISTRY

PAPER

View Article Online
View Journal

Cite this: DOI: 10.1039/d5en00955c

Predicting skin irritation, corrosion, and sensitization potential of nanomaterials using OECD-validated new approach methodologies (NAMs)

Olivia Lautan,†[a] Yu-Ying Chen,[a] Yung-Hsuan Cheng,†[a] Ssu-Ning Chen,[b] Hsiu-Ling Chen,[b] Hsien-Jen Cheng,[c] Rong-Jane Chen *[b] and Ying-Jan Wang*[ad]

Received 15th October 2025,
Accepted 7th May 2026

DOI: 10.1039/d5en00955c

rsc.li/es-nano

Nanomaterials are increasingly used in consumer and industrial products, creating a need for comprehensive and reliable safety evaluations. Current standardized methods developed by the Organisation for Economic Co-operation and Development (OECD) have yet to be fully validated for the assessment of nanomaterials. This study systematically investigated the skin irritation, corrosion, and sensitization potential of five industrially relevant nanoparticles (NPs): titanium dioxide (TiO_2), zinc oxide (ZnO), nickel oxide (NiO), silver (Ag), and polystyrene (PS), using OECD-validated *in vitro* models and the integrated approach to testing and assessment (IATA). The reliability of OECD Test Guidelines (TGs) 439 and 431 for assessing nanomaterials-induced skin irritation and corrosion was confirmed, with results integrated using the IATA framework as outlined in OECD Guidance Document 203. However, skin sensitization assays, including KeratinoSens™ (TG 442D), the human Cell Line Activation Test (h-CLAT, TG 442E), and the Defined Approaches (Guideline 497), produced conflicting or inconclusive results for certain metal-based NPs such as TiO_2 and NiO, while Ag NPs consistently tested positive across multiple assays. The 3D reconstructed human epidermis (RHE) model for skin irritation and corrosion testing minimised assay interference and provided a more physiologically relevant representation of the skin barrier compared with conventional 2D cultures used in skin sensitization assays. This study highlights the applications and limitations of existing OECD TGs and current *in vitro* approaches for evaluating potential skin toxicities of metal-based NPs. By identifying current gaps, it supports refinement of reliable, standardized non-animal testing strategies and informs future adaptation of regulatory guidelines for improved nanomaterials safety assessment.

Environmental significance

The growing use of nanomaterials (NMs) in consumer and industrial products raises concerns for human and environmental health, highlighting the need for standardized safety testing. Current OECD Test Guidelines (TGs) are not fully validated for NMs assessment. We systematically evaluated five industrially relevant NMs using OECD-approved *in vitro* models within the IATA and DA frameworks. OECD TGs were reliable for assessing skin irritation and corrosion but produced inconsistent results for some metal-based NPs in skin sensitization assays. These findings reveal critical gaps in current approaches and support the refinement of OECD TGs to deliver more reliable, non-animal testing strategies.

Introduction

The widespread application of nanotechnology in recent decades has enabled mass production of nanomaterials across various chemical types, integrating them into many consumer and industrial products.[1,2] Nanomaterials, including nanoparticles (NPs), commonly defined as materials with nanoscale dimensions, share unique physicochemical properties that often yield novel or enhanced functionalities compared with conventional materials of the same composition.[3,4] To ensure the safety of

[a] *Department of Environmental and Occupational Health, College of Medicine, National Cheng Kung University, 138 Sheng-Li Road, Tainan 70428, Taiwan. E-mail: yjwang@mail.ncku.edu.tw; Fax: +886 6 275 2484; Tel: +886 6 235 3535 Ext. 5804*
[b] *Department of Food Safety/Hygiene and Risk Management, College of Medicine, National Cheng Kung University, 138 Sheng-Li Road, Tainan 70428, Taiwan. E-mail: janekhc@gmail.com*
[c] *National Center for Biomodels, National Institutes of Applied Research, Taipei, Taiwan*
[d] *Department of Medical Research, China Medical University Hospital, China Medical University, Taichung, Taiwan*
† Olivia Lautan and Yung-Hsuan Cheng contributed equally to this work.

products containing nanomaterials, it is crucial to assess their potential risks to human health and the environment, considering their increasing release into environmental systems and the resulting human exposure through occupational pathways such as workplace handling and production, as well as consumer-related pathways including dietary exposure, migration from packaging, cosmetics, and other everyday products.[5,6] Traditional hazard assessment methods largely follow Organisation for Economic Co-operation and Development (OECD) guidelines but often rely on animal testing.[7,8] The diversity of nanomaterials sizes, shapes, surface coatings, and compositions makes comprehensive *in vivo* testing impractical. New approach methodologies (NAMs) have therefore been developed to provide more efficient, ethical, and mechanistic methods for assessing nanomaterials safety.[8,9] NAMs include *in silico*, *in chemico*, and *in vitro* alternative test methods used individually or in combination to predict the hazardous properties of chemicals, supporting high-throughput screening and providing mechanistic insights into toxicity while reducing reliance on animal testing.[8,10]

Despite rapid advancements in the development of NAMs, a key challenge remains: increasing scientific confidence in these methods and effectively integrating them into regulatory decision-making frameworks.[8] Several NAMs have been validated by the OECD for assessing local toxicity endpoints, including skin sensitization, irritation, corrosion, and phototoxicity, and their results can be incorporated into integrated approaches to testing and assessment (IATA) framework.[11,12] For skin irritation and corrosion assessment, reconstructed human epidermis (RHE) models, which are three-dimensional (3D) human skin equivalents derived from non-transformed keratinocytes, have become widely accepted alternatives. Commercial RHE models such as EpiDerm™, EpiSkin™, and SkinEthic™ closely mimic key structural and functional properties of human skin,[13,14] and have been adopted into OECD test guidelines (TGs) 431 (*In Vitro* Skin Corrosion)[15] and 439 (*In Vitro* Skin Irritation),[16] along with the IATA concept outlined in OECD Guidance Document (GD) 203, which provides a classification framework based on the United Nations Globally Harmonized System (UN GHS) of Classification and Labelling of Chemicals.[17] For skin sensitization, OECD TGs 442C, 442D, and 442E address the first three key events (KEs) of the adverse outcome pathway (AOP) of allergic contact dermatitis.[18,19] The first KE involves covalent binding of electrophilic chemicals to nucleophilic centres of skin proteins.[20] The second KE includes activation of inflammatory responses and the antioxidant/electrophile response element (ARE) pathway in human keratinocytes, assessed using the ARE-Nrf2 Luciferase KeratinoSens™ test.[21] The third KE involves the expression of CD86 and CD54 membrane markers in human THP-1 monocyte cells, evaluated using the human Cell Line Activation Test (h-CLAT).[22] These methods have been incorporated into defined approaches (DAs) for skin sensitization, as described in OECD Guideline 497,[23] 23 which includes the "2 out of 3" (2o3) approach that combines results from the DPRA, KeratinoSens™, and h-CLAT assays. This demonstrates how limitations of individual *in vitro* methods can be addressed by integrating multiple NAMs, thereby improving overall reliability and confidence in safety assessments.

While these standardized NAMs have proven effective for many conventional chemicals, their applicability to nanomaterials remains uncertain.[24] Recognizing these differences, the OECD Working Party on Manufactured Nanomaterials (WPMN) has proposed key properties for nanomaterials characterization,[25] including particle size, size distribution, and specific surface area, which are addressed in OECD TGs relevant to nanomaterials, such as TG 124, 125, and 126.[26–28] Yet the unique behaviors of nanomaterials, such as their tendency to agglomerate in suspension or interact with test media and assay components, can affect the performance and reliability of *in vitro* OECD TGs and GDs,[4,5,29] highlighting the need for adaptation of these guidelines to minimize potential biases and artifacts.[4,30] Metal, metal oxide, and polystyrene-based NPs are widely used in industrial, biomedical, and cosmetic applications, and their incorporation into topical formulations can enhance delivery through the skin due to small size and high surface area.[31,32] However, accumulating evidence shows that NPs can exert cytotoxic effects after skin penetration.[33–35] Although NPs are typically considered minimally soluble under normal physiological conditions, their solubility can increase under specific conditions, such as in acidic lysosomal fluid. In such environments, certain NPs have demonstrated significant dissolution.[32,36,37] In these cases, toxicity may be linked to the intrinsic toxicity of released metal ions rather than the NPs themselves. Currently, there is limited information on the effectiveness of established guidelines for assessing the skin toxicity of nanomaterials, including irritation, corrosion, and sensitization.[36] Moreover, with the growing emphasis on animal welfare, the applicability of NAMs for assessing nanomaterials toxicity has emerged as a critical research focus.

In this study, we selected five NPs that are commonly encountered through skin contact and hold industrial significance: titanium dioxide (TiO_2) NPs, widely used in cosmetic formulations such as sunscreens for their UV-blocking properties;[38] zinc oxide (ZnO) NPs, used in skincare products, coatings, and paints;[39] nickel oxide (NiO) NPs, applied in batteries, catalysts, and electronic components;[40] silver (Ag) NPs, valued for their antimicrobial properties in medical devices, wound dressings, and textiles;[41] and polystyrene (PS) NPs, frequently used in biomedical research as model particles due to their high stability and ease of functionalization.[42] These NPs are encountered across a range of exposure scenarios, including occupational dermal contact during manufacturing or handling,[43] intentional skin application in consumer and medical products,[44,45] and indirect environmental exposure through release into wastewater systems following product

use.[46] PS NPs in particular have gained significant attention as emerging environmental contaminants derived from the degradation of plastic waste, contributing to growing concerns over microplastics and nanoplastics in environmental systems. Despite their ubiquity and the rising concerns regarding microplastics and nanoplastics exposure, data on their skin toxicity remain limited.[47,48] Our goal is to generate data to evaluate whether existing OECD guidelines, including TG 439 and TG 431 for skin irritation and corrosion and TG 442D and TG 442E for skin sensitization, are suitable for testing the skin toxicity of nanomaterials. For comparison, we also included the bulk form of titanium dioxide (bulk TiO_2), larger polystyrene microparticles (PS MPs), and the ionic forms of ZnO NPs, NiO NPs, and Ag NPs. These comparisons aim to clarify the distinct behaviors and toxicological profiles of nanoscale materials relative to their bulk counterparts and to examine the hypothesized toxicity of metal NPs attributed to released metal ions.

For skin irritation and corrosion, we used the EPiTRI model, a 3D reconstructed human epidermis (RHE) system developed by the Industrial Technology Research Institute (ITRI), Taiwan, and validated under OECD TG 439,[49] together with the IATA framework outlined in OECD GD 203. For skin sensitization, we used the KeratinoSens™ and h-CLAT assays, in line with OECD TGs 442D and 442E, and applied the defined approaches described in OECD GD 497. Our findings provide insight into the applicability of OECD TGs 439 and 431, along with GD 203, for assessing the skin irritation and corrosion potential of nanomaterials. Our results also highlight the need for further refinement and validation of *in vitro* skin sensitization models to ensure their reliability for nanomaterials safety assessment. Overall, these findings contribute to ongoing efforts to adapt OECD guidelines to account for the unique properties of nanomaterials and to improve their regulatory acceptance in safety assessment frameworks.

Materials and methods

Chemicals and reagents

Titanium dioxide (TiO_2) and zinc oxide (ZnO) nanoparticles (NPs) were generously provided by the JRC Nanomaterials Repository (Italy). Nickel oxide (NiO) and silver (Ag) NPs were sourced from US Research Nanomaterials, Inc. (USA). Polystyrene (PS) NPs (size <100 nm) and corresponding PS microparticles (size ~1 μm), TiO_2 (bulk form), nickel(II) nitrate hexahydrate ($Ni(NO_3)_2{\cdot}6H_2O$), and zinc nitrate ($Zn(NO_3)_2{\cdot}6H_2O$) were purchased from Sigma-Aldrich (USA). Silver nitrate ($AgNO_3$) was obtained from Honeywell International Inc. (USA). Dulbecco's modified Eagle medium (DMEM) and fetal bovine serum (FBS) were acquired from Gibco, Thermo Fisher Scientific (USA). G418 was sourced from BioBasic (USA). L-Glutamine, RPMI-1640, and sodium pyruvate were purchased from Simply, GeneDireX Inc. (Taiwan). Passive lysis buffer and modified luciferase substrate for h-CLAT assay were obtained from Promega (Germany). PE-labeled anti-CD86 antibodies and APC-labeled anti-CD54 antibodies were sourced from BD Pharmingen (USA).

Preparation and characterization of NPs suspensions

NPs in dry powder form were weighed and dispersed in Milli-Q water at 1 mg mL^{-1}, then sonicated for 20 minutes using a bath-type sonicator (D80H, DELTA, Taiwan). Fresh stock suspensions were prepared immediately before dosing tissues or cells. NPs morphology and primary particle size were determined by transmission electron microscopy (TEM; JEM-2100F, JEOL, Japan). Hydrodynamic diameter, polydispersity index (PDI), and zeta potential were measured by dynamic light scattering (DLS; Delsa™ Nano C, Beckman Coulter, USA). Elemental composition was confirmed using energy-dispersive X-ray spectroscopy (EDS; JSM-7100F, JEOL, Japan). Surface area was analyzed with a BET surface area analyzer (ASAP 2060, Micromeritics, USA). Metal ion release was quantified by inductively coupled plasma mass spectrometry (ICP-MS; Element XR, Thermo Fisher Scientific, USA). For this, fresh NPs suspensions were prepared at the highest tested concentration (1 mg mL^{-1}) in ultrapure Milli-Q water, incubated for 30 or 60 minutes to match *in vitro* skin irritation and corrosion exposure times. The suspensions were centrifuged to pellet any insoluble NPs, and the supernatant was collected for ICP-MS quantification of released metal ions.

Reconstructed human epidermis (RHE) model EPiTRI

The EPiTRI RHE models (EPiTRI-SIT for irritation, EPiTRI-SCT for corrosion) were obtained from the Industrial Technology Research Institute (ITRI, Taiwan). Each lot met OECD TG 439 and TG 431 performance standards for barrier function, histological integrity, sterility, and antigen-free conditions.

i. Interference test for skin irritation/corrosion assay. Prior to irritation and corrosion assays, an interference test was performed following OECD TGs 439 and 431 to assess whether the test substances reduced 3-(4,5-dimethylthiazol-2-yl)-2,5-diphenyltetrazolium bromide (MTT; Thermo Fisher Scientific, USA) directly or caused color interference. Each substance was incubated with deionized water at 37 °C with 5% CO_2 for 60 minutes. Mixtures were shaken and inspected for color changes that could affect absorbance measurements.

ii. *In vitro* skin irritation assay (OECD TG 439). The protocol used in this study followed the procedures described in the peer-reviewed validation paper.[49] Upon arrival, tissues were transferred to culture medium and allowed to reconstitute overnight. Tissues were then treated with each test substance (35 ± 1 μL for liquids; 25 ± 1 mg for solids), a negative control (phosphate-buffered saline, PBS), and a positive control (5% aqueous sodium dodecyl sulfate, SDS). NPs and their corresponding materials were applied either as dry powders or as 1 mg mL^{-1} suspensions prepared in Milli-Q

water. All treatments were performed in three biological tissue replicates as required by OECD TG 439. Following a 30 minute exposure period, tissues were rinsed thoroughly with PBS to remove any residual test substance. Tissues were then transferred to fresh culture medium for a post-exposure incubation of approximately 42 hours to assess the potential for recovery, with a medium change after 24 hours. After the recovery period, cell viability was determined using the MTT assay: tissues were incubated with MTT solution (1 mg mL^{-1}) for 3 hours at 37 °C. Formazan crystals formed in viable cells were then extracted with isopropanol for an additional 3 hours under sealed conditions to prevent evaporation. From each tissue replicate, two 200 μL aliquots of the formazan extract were transferred to a 96-well plate, and the optical density was measured at 570 nm (OD570) using a microplate reader (Multiskan EX, Thermo Fisher Scientific, USA). The two OD readings per tissue were averaged to obtain a single mean OD per tissue replicate. Relative tissue viability for each treatment group was compared to the negative control group and expressed as a percentage (%). According to UN GHS classifications criteria, test substances resulting in a reduction of viability to ≤50% were classified as irritants, whereas substances with viability >50% were classified as non-irritants.

iii. *In vitro* skin corrosion assay (OECD TG 431). Tissue preparation followed procedures similar to those of the *in vitro* skin irritation assay, with slight differences in exposure time and the absence of a post-exposure recovery period. Test substances (35 ± 1 μL for liquids; 25 ± 1 mg for solids) were applied for exposure periods of 3 and 60 minutes. An 8N potassium hydroxide (KOH) solution was used as the positive control for the 60 minute exposure time, in accordance with the protocol provided by ITRI. NPs and their corresponding materials were applied either as dry powders or as 1 mg mL^{-1} suspensions prepared in Milli-Q water. All treatments were performed in two biological tissue replicates, as required by OECD TG 431. Following exposure, tissues were rinsed thoroughly with PBS and immediately subjected to the MTT assay (1 mg mL^{-1}) without further incubation. From each tissue replicate, two 200 μL aliquots of the extracted formazan solution were transferred into a 96-well plate, and the mean OD570 values were measured using a microplate reader. Relative tissue viability for each treatment group was compared to the negative control group and expressed as a percentage (%). According to UN GHS classification criteria, substances that reduced tissue viability to ≤50% after the 3 minute exposure or to ≤15% after the 60 minute exposure were classified as corrosive.

iv. Acceptance criteria. For the EPiTRI-SIT model, the assay was considered valid when the following criteria were met. The mean OD570 of the negative control tissues treated with PBS was between 1.0 and 1.8. The mean relative viability of the positive control (5% SDS) was ≤20% of the negative control. In addition, the standard deviation of the relative tissue viability among the three biological replicates for each treatment did not exceed 18%. For the EPiTRI-SCT model, the assay was accepted when the mean OD570 of the negative control tissues treated with deionized water was between 0.8 and 3.0 at each exposure time. The mean relative viability of the positive control (8N KOH) was <15% of the negative control after 60 minutes of exposure. When two tissue replicates were used per exposure time, the difference in relative viability between the two replicates did not exceed 30%.[49]

KeratinoSens™ assay (OECD TG 442D)

This assay was used to evaluate the second key event (KE) in the AOP for skin sensitization: keratinocyte activation. The immortalized human keratinocyte cell line transfected with the KeratinoSens™ plasmid (acCELLerate GmbH, Germany) was cultured in DMEM supplemented with 4.5 g L^{-1} glucose, 2% L-glutamine, 10% FBS, and 500 μg mL^{-1} G418. Prior to testing, cells were seeded into 96-well plates (clear for cytotoxicity; white for luciferase activity) at 10 000 cells per well and adapted to G418-free medium for 24 hours. Cells were exposed for 48 hours to 12 concentrations of each test substance. For NPs and bulk particles without defined molecular weights, the concentration range was 0.195 to 400 μg mL^{-1}, while for remaining corresponding materials, the range was 0.98 to 2000 μM. Following incubation, cells were lysed with passive lysis buffer, and luminescence was measured with a modified luciferase substrate using a luminometer (Luminoskan, Thermo Fisher Scientific, USA). The signal was integrated for 2 seconds. Fold luciferase induction was calculated as:

$$\text{Fold induction} = (L_{\text{sample}} - L_{\text{blank}})/(L_{\text{solvent}} - L_{\text{blank}})$$

The EC1.5 value was determined by linear interpolation:

$$\text{EC1.5} = (C_b - C_a) \times \left(\frac{1.5 - I_a}{I_b - I_a}\right) + C_a$$

where C_a and C_b are the lowest and highest concentrations with >1.5- and <1.5-fold induction, respectively; I_a and I_b as their corresponding mean fold induction values (mean of three replicates). Cell viability was determined by MTT assay (0.5 mg mL^{-1}) following a 1 hour incubation at 37 °C with 5% CO_2. OD570 was measured with a microplate reader, and viability was calculated as:

$$\text{Viability} = \frac{(V_{\text{sample}} - V_{\text{blank}})}{(V_{\text{solvent}} - V_{\text{blank}})} \times 100\%$$

Human cell line activation test (h-CLAT) assay (OECD TG 442E)

This assay was performed to assess the third KE: dendritic cell activation. Human THP-1 monocytes (BCRC, Taiwan) were maintained in RPMI-1640 medium supplemented with 10% FBS and 5% sodium pyruvate. For testing, 1 × 10^6 cells per well were seeded in 12-well plates and exposed for 24 hours to 8 serial dilutions of each test substance (1.2-fold dilution series). Following treatment, cells were washed with

PBS, blocked with 1% FBS for 15 minutes, and stained with PE-labeled anti-CD86, APC-labeled anti-CD54 antibodies, and propidium iodide (PI) for 30 minutes at room temperature. Stained cells were analyzed by flow cytometry (CytoFlex, Beckman Coulter, USA). Relative fluorescence intensity (RFI) was calculated as:

$$\mathrm{RFI} = \frac{(\text{MFI of chemical-treated cells} - \text{MFI of chemical-treated isotype control cells})}{(\text{MFI of solvent-treated control cells} - \text{MFI of solvent-treated isotype control cells})} \times 100$$

Cell viability was assessed using PI staining:

$$\text{Viability} = \frac{\text{Number of living cells}}{\text{Total Number of acquired cells}} \times 100$$

Good *in vitro* method practices (GIVIMP) alignment

The experimental methods in this study were performed in alignment with the OECD Guidance Document on good *in vitro* method practices (GIVIMP) to ensure the generation of reliable, robust, and reproducible data.[50] Throughout the assessment, good scientific, technical, and quality practices were applied, including the use of validated 3D RHE models and cell lines that met mandatory quality control standards for barrier function, histological integrity, and sterility. All procedures followed established Standard Operating Procedures (SOPs) based on OECD TGs, performed by trained personnel to maintain scientific integrity and consistency across multiple independent runs. A key component of this alignment involved the proactive identification and mitigation of test item-test system interactions; specifically, methodological adaptations such as background absorbance calibration and specialized cell-tracer gating strategies were implemented to correct for NPs-induced interference in colorimetric and fluorescent readouts. Furthermore, the inclusion of concurrent positive and negative controls confirmed the sensitivity of the test systems, confirming the overall validity of the results.

Statistical analysis

Statistical analyses were performed using an unpaired two-tailed Student's *t*-test. Results are presented as mean ± standard deviation (mean ± SD). A p-value <0.05 was considered statistically significant.

Results

Physicochemical characterization of nanoparticles

In this study, the main globally accepted guidelines considered for the sample preparation of NPs and the characterization of their physicochemical properties are based on recommendations outlined in OECD TG 125 (ref. 27) and the OECD Series on the Safety of Manufactured Nanomaterials, No. 36 (ref. 51) and No. 63.[52] The characterization results are summarized in Table 1. The morphology and primary size of five selected NPs were analyzed using transmission electron microscopy (TEM) and all five NPs exhibited predominantly spherical morphology (Fig. 1), and the primary particle sizes varied from NiO NPs being the smallest (12.65 ± 2.58 nm) to PS NPs the largest (79.46 ± 12.32 nm). Dynamic light scattering (DLS) measurements provided insight into the hydrodynamic diameter, revealing that TiO_2 and ZnO NPs exhibited relatively large hydrodynamic sizes (~171–178 nm), while Ag NPs had the smallest hydrodynamic diameter (~65.4 nm). The low polydispersity index (PDI) values showed that these NPs have a high degree of uniformity in particle dispersion. Zeta potential analysis showed that ZnO and NiO NPs had positive surface charges (+28.12 mV and +37.75 mV, respectively), whereas TiO_2, PS, and Ag NPs carried negative charges (−20.96 mV, −30.71 mV, and −25.12 mV, respectively). The specific surface areas of the NPs were determined as 45.19 ± 0.09 $m^2\ g^{-1}$ (TiO_2 NPs), 73.24 ± 10.64 $m^2\ g^{-1}$ (PS NPs), 8.85 ± 0.05 $m^2\ g^{-1}$ (ZnO NPs), 72.64 ± 0.80 $m^2\ g^{-1}$ (NiO NPs), and 0.05 ± 0.02 $m^2\ g^{-1}$ (Ag NPs). Collectively, these results confirm that the selected NPs possess key nanoscale properties relevant to nanotoxicology studies, including size, morphology, surface charge, and surface area.

Skin irritation/corrosion potency using top-down approach

A critical aspect of our study was assessing whether NPs in their original powder form or as suspensions induce different skin irritation and corrosion effects. We also examined whether these effects were caused by the NPs themselves or

Table 1 Physicochemical characterization of the five selected nanoparticles

NPs physicochemical properties	TiO_2 NPs	PS NPs	ZnO NPs	NiO NPs	Ag NPs
Primary size (nm)	21.02 ± 8.24	79.46 ± 10.32	55.09 ± 18.84	12.65 ± 2.58	58.33 ± 4.63
Hydrodynamic diameter (nm)	178 ± 49.4	88.6 ± 18.1	171.5 ± 47.4	159.9 ± 44.7	65.4 ± 8.1
Polydispersity index (PDI)	0.274	0.027	0.183	0.242	0.212
Zeta potential (mV)	−20.96	−30.71	28.12	37.75	−25.12
Surface area ($m^2\ g^{-1}$)	45.19 ± 0.09	73.24 ± 10.64	8.85 ± 0.05	72.64 ± 0.80	0.05 ± 0.02
Elemental composition	O, Ti	C	Zn, O	O, Ni	Ag
Released metal ions in 1 mg mL^{-1} NPs suspension (μg mL^{-1})	Non-detected	Non-metal	30 min: 5.385 60 min: 5.412	30 min: 3.181 60 min: 3.218	30 min: 0.057 60 min: 0.072

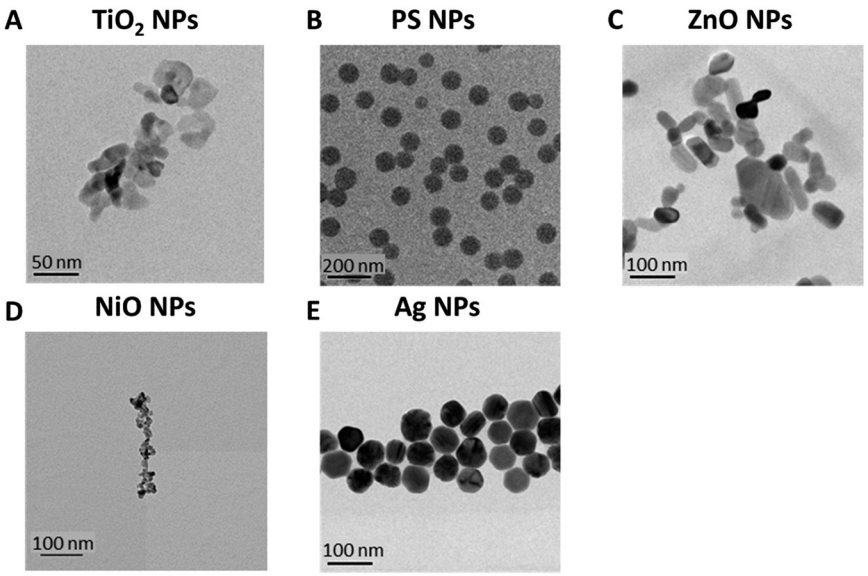

Fig. 1 Morphology of the selected NPs observed using transmission electron microscopy (TEM). Representative TEM images of the five NPs: (A) TiO_2 NPs, (B) PS NPs, (C) ZnO NPs, (D) NiO NPs, and (E) Ag NPs. Scale bars: 50–200 nm.

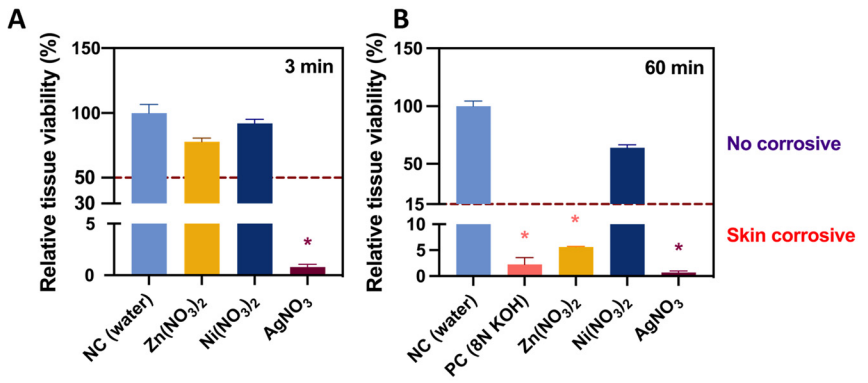

C

Top-down approach: Skin corrosion results (Original powder form)			
Test substance	Relative tissue viability (%)		UN GHS Classification
	3 min.	60 min.	
$Zn(NO_3)_2$	77.8 ± 2.9	5.6 ± 0.1	Category 1B/C: skin corrosive
$Ni(NO_3)_2$	92.0 ± 3.0	65.2 ± 1.5	No category: Not corrosive
$AgNO_3$	0.7 ± 0.1	0.7 ± 0.3	Category 1A: Skin corrosive
Water (NC)	100.0 ± 6.7	100.0 ± 4.3	No category
8N KOH (PC)	-	3.0 ± 0.4	Skin corrosive

D

OECD TG 431 skin corrosion assay (EPiTRI-SCT model)	
Relative tissue viability (%)	Predicted UN GHS classification
Exposure for 3 min < 50%	Category 1A: Skin corrosive
Exposure 3 min ≥ 50% and 60 min < 15%	Category 1B/1C: Skin corrosive
Exposure 3 min ≥ 50% and 60 min > 15%	No category: not skin corrosive

Fig. 2 Skin corrosion results of the corresponding materials based on top-down approach. Quantification of relative tissue viability after (A) 3 minutes and (B) 60 minutes exposure to zinc nitrate, nickel nitrate, and silver nitrate. (C) UN GHS classification of the test substances according to the relative tissue viability. (D) Prediction model for skin corrosion assay according to OECD TG 431. Mean ± S.D ($n \geq 3$); * p-value ≤ 0.05 compared to control.

by the toxicity of their released metal ions. Skin irritation and corrosion testing were conducted in accordance with OECD GD 203 on the IATA for skin corrosion and irritation. According to the guidance, substances with sufficient weight of evidence (WoE) indicating potential irritant or corrosive properties are tested using a top-down approach, beginning with the skin corrosion test (OECD TG 431). Three of the corresponding materials: nickel(II) nitrate hexahydrate ($Ni(NO_3)_2{\cdot}6H_2O$), zinc nitrate ($Zn(NO_3)_2{\cdot}6H_2O$), and silver nitrate ($AgNO_3$), had existing evidence suggesting their potential to induce skin irritation or corrosion. The results demonstrated that only silver nitrate induced skin corrosion, as indicated by a significant reduction in tissue viability (<50%) after just 3 minutes of exposure (Fig. 2A). At the 60 minute exposure point, both silver nitrate and zinc nitrate reduced tissue viability to below 15% (Fig. 2B). Based on these results, silver nitrate was classified as category 1A for skin corrosion, while zinc nitrate was classified as category 1B (Fig. 2C). Nickel nitrate did not exhibit corrosive properties and will undergo further testing in the skin irritation assay to assess its potential to induce irritation.

Skin irritation/corrosion potency using bottom-up approach

The remaining seven test substances, including five NPs: TiO_2 NPs, PS NPs, ZnO NPs, NiO NPs, and Ag NPs, along with two corresponding materials, bulk TiO_2 and PS microparticles (PS MPs), lacked sufficient weight of evidence (WoE) indicating skin irritation or corrosion. As per OECD GD 203, these substances were tested using the bottom-up approach, starting with the skin irritation assay (OECD TG 439). Following 30 minutes of exposure and approximately 42 hours of recovery, none of the seven substances reduced relative tissue viability to below 50%. However, nickel nitrate, previously tested in the top-down approach, significantly reduced tissue viability to below 50%, indicating skin irritation potential. Additionally, the two substances previously classified as corrosive (silver nitrate and zinc nitrate) were retested in the skin irritation assay. Both substances further decreased tissue viability, confirming their corrosive properties (Fig. 3A). Based on these results, nickel nitrate was classified as a category 2 skin irritant, while the remaining seven substances, even in their original powder form, were classified as non-irritants (no category) under UN-GHS guidelines (Fig. 3B).

Additionally, we also assessed the skin irritation and corrosion potential of the NPs and their corresponding materials as 1 mg mL^{-1} suspensions. Bulk TiO_2 and PS MPs were tested at the same concentration, and for metal-based NPs, the released metal ion concentrations were measured using ICP-MS (Table 1) and used in the assays. None of the test substances caused relative tissue viability to drop below 50% (Fig. S1B and C), consistent with the results observed for the original forms.

Nanoparticles interference in KeratinoSens™ assay and h-CLAT assay

In the KeratinoSens™ assay, MTT is used to measure cell viability after 48 hours of exposure. To investigate NPs-induced interference with MTT measurements, cell viability was calculated without interference calibration. The results showed that TiO_2 NPs significantly increased viability (up to 200%) at 400 μg mL^{-1}, indicating interference with absorbance measurements (Fig. 4A). Background absorbance values of NPs combined with cells, measured at 570 nm, increased with NPs concentration. After calibrating for background interference, the viability no longer increased with concentration (Fig. 4B). Similar interference effects were observed for NiO NPs and Ag NPs (Fig. 4C and E), and background-calibrated viability was calculated accordingly (Fig. 4D and E).

In the h-CLAT assay, the fluorescence intensity of CD86 and CD54 is measured by flow cytometry. To assess

A

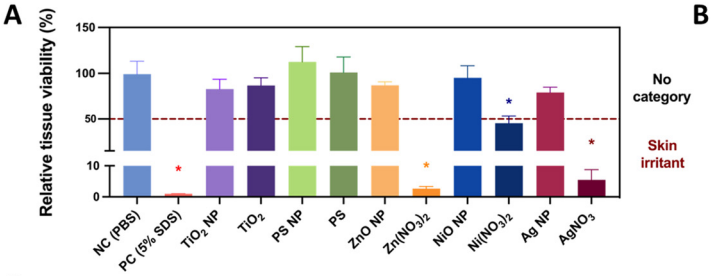

B

Bottom-up approach: Skin irritation results (Original powder form)			
Test substance		Relative tissue viability (%)	UN GHS Classification
NPs	TiO_2 NPs	82.9 ± 10.7	No category
	PS NPs	112.6 ± 16.3	No category
	ZnO NPs	87.6 ± 3.8	No category
	NiO NPs	95.9 ± 13.3	No category
	Ag NPs	81.0 ± 5.3	No category
Corresponding materials (bulks or metal ions)	TiO_2	87.4 ± 8.5	No category
	PS	100.9 ± 16.7	No category
	$Zn(NO_3)_2$	2.7 ± 0.7	Skin irritant*
	$Ni(NO_3)_2$	45.4 ± 7.9	Category 2: Skin irritant
	$AgNO_3$	5.6 ± 3.2	Skin irritant*
PBS (NC)		100.0 ± 12.7	No category
5% SDS (PC)		1.0 ± 0.4	Skin irritant

C

OECD TG 439 skin irritation assay (EPiTRI-SIT model)	
Relative tissue viability (%)	Predicted UN GHS classification
Exposure 30 min + post-incubation ≤ 50%	Category 2: skin irritant
Exposure 30 min + post-incubation > 50%	No category: not skin irritant

Fig. 3 Skin irritation results of NPs and their corresponding materials based on bottom-up approach. (A) Quantification of relative tissue viability after 30 minutes exposure to all the test substances. (B) UN GHS classification of the test substances according to the relative tissue viability. (C) Prediction model for skin irritation assay according to OECD TG 439. Mean ± S.D ($n \geq 3$); * p-value ≤0.05 compared to control.

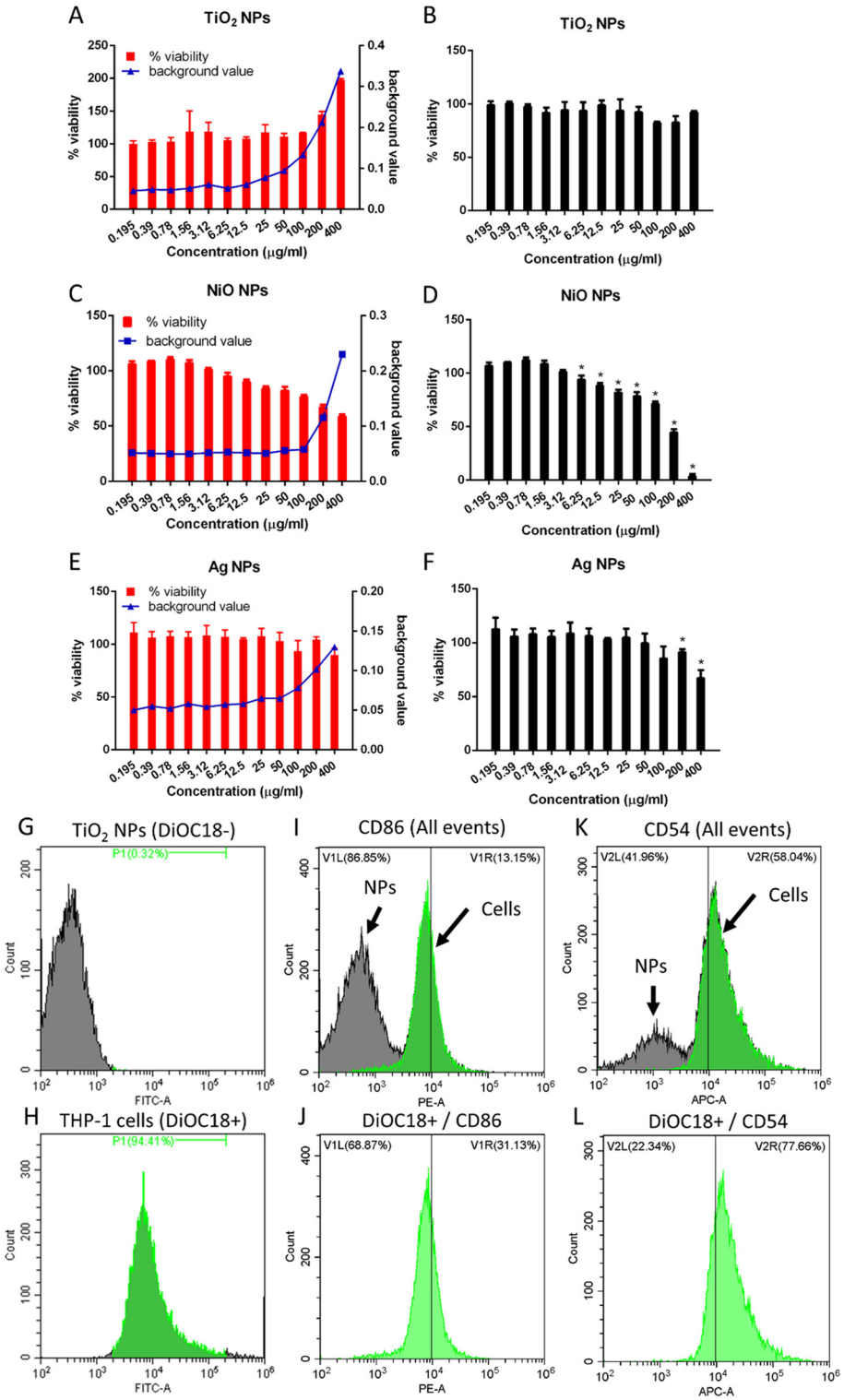

Fig. 4 Cell viability interference of NPs in the KeratinoSens™ assay and fluorescence interference of NPs in h-CLAT assay. Dose response curve of cell viability and background value of (A) TiO_2 NPs, (C) NiO NPs, and (E) Ag NPs. Cell viability after background valve calibration of (B) TiO_2 NPs, (D) NiO NPs, and (F) Ag NPs. Influence of NPs in cell count and fluorescence intensity in flow cytometry analysis. (G and H) THP-1 cells were first stained with DiOC18 dye then treated with NPs. The histogram indicated subgroups of NPs and cells can be separated at FITC channel. (I and J) Histogram of CD86 with or without calibration of NPs fluorescence interference by using DiOC18 label method. (K and L) Histogram of CD54 with or without calibration of NPs fluorescence interference by using DiOC18 label method. Mean ± S.D ($n \geq 3$); * p-value ≤0.05 compared to control.

fluorescence interference caused by NPs, our results showed that NPs generated intrinsic fluorescence signals, which interfered with the detection of cellular fluorescence signals. CD86 and CD54 expression were measured using PE and APC fluorescence. With NPs interference, the results indicated that NPs-generated fluorescence reduced the MFI for both CD markers. This interference significantly impacted the prediction of h-CLAT conclusions. To address this problem, DiOC18, a cell tracer dye, was applied 24 hours prior to NPs exposure. After exposure, the medium was replaced with fresh medium, and the NPs exposure procedure continued. This step enabled the separation of cellular fluorescence signals from NPs fluorescence using FITC-green fluorescence from the cell tracer dye (Fig. 4G and H). Following the cell gating process, the MFI of CD86 and CD54 for cells alone was calculated accordingly (Fig. 4I–L). This additional cell staining step will be applied in subsequent h-CLAT assays for NPs-exposed groups.

Skin sensitization potency using KeratinoSens™ assay

Before conducting routine KeratinoSens™ assays, cinnamic aldehyde was used as a PC to verify the acceptance criteria of the assay. Results from the cinnamic aldehyde group demonstrated statistically significant luciferase activity induction above the 1.5-fold threshold (EC1.5) at concentrations ranging from 4 to 64 μM. The maximum fold induction (I_{max}) observed at 64 μM was 2.49 (Fig. S2A). These results met the acceptance criteria outlined in the OECD TG 442D and confirmed the validity of the subsequent tests.[21]

We found that PS NPs, PS MPs, and bulk TiO_2 did not induce luciferase activity exceeding the EC1.5 threshold at any concentration tested (Fig. 5A). According to the prediction model outlined in OECD TG 442D, these results were classified as negative for skin sensitization potential (Fig. 5F). ZnO NPs induced luciferase activity ranging from 1.35- to 1.67-fold at concentrations between 0.8 and 50 μg

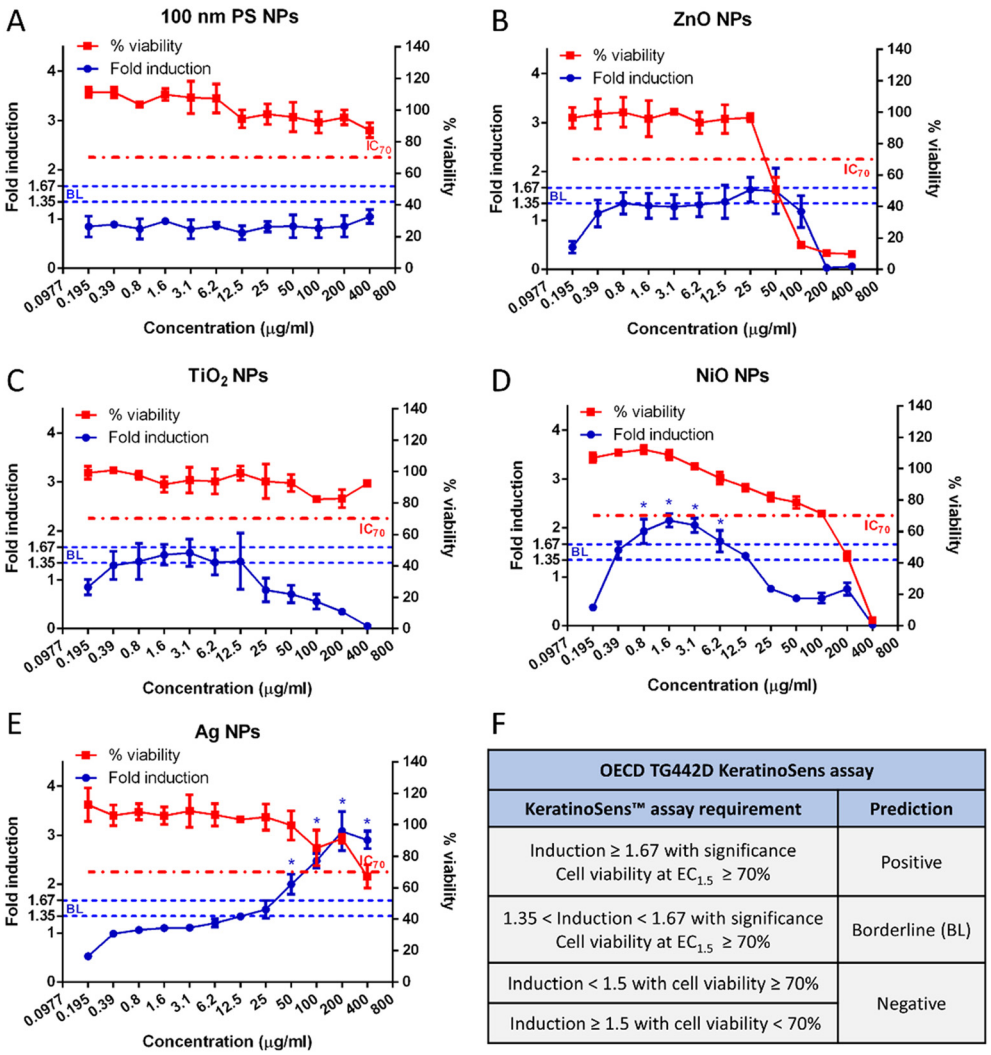

Fig. 5 KeratinoSens™ assay results of five types of nanoparticles. Dose response curve of luciferase activity induction and cell viability changes of (A) PS NPs, (B) ZnO NPs, (C) TiO_2 NPs, (D) NiO NPs, and (E) Ag NPs. (F) Prediction model of KeratinoSens™ assay according to OECD TG 442D. Mean ± S.D ($n \geq 3$); * p-value ≤0.05 compared to control.

mL^{-1}, while TiO_2 NPs exhibited similar activity levels at concentrations between 0.39 and 12.5 μg mL^{-1} (Fig. 5B and C). Based on the prediction model, these results were classified as borderline, requiring additional assays to confirm their sensitization potential (Fig. 5F). NiO NPs showed a maximum fold luciferase induction of 2.15 at 1.6 μg mL^{-1}, while Ag NPs exhibited a maximum induction of 3.38 at 200 μg mL^{-1} (Fig. 5D and E). Consequently, both NiO and Ag NPs were classified as positive for skin sensitization potential (Fig. 5F).

To determine whether the observed skin sensitization effects originated from the NPs themselves rather than from released ions or bulk materials, the corresponding ions and bulk forms were also tested using the KeratinoSens™ assay. Neither 1 μm PS MPs nor Bulk TiO_2 induced luciferase activity exceeding the EC1.5 at any concentration (Fig. 6A and C), resulting in negative predictions for both materials. In contrast, nickel nitrate ($Ni(NO_3)_2$) induced a maximum fold induction of 1.7 at 250 μM, zinc nitrate ($Zn(NO_3)_2$) induced 1.95-fold induction at 31.25 μM, and silver nitrate ($AgNO_3$) induced a striking 22.05-fold induction at 125 μM. Therefore, these three corresponding ionic forms were classified as positive for skin sensitization based on their KeratinoSens™ results.

Skin sensitization potency using h-CLAT assay

Before conducting routine h-CLAT assays, 2,4-dinitrochlorobenzene (DNCB) was used as a PC to confirm that the assay met the acceptance criteria outlined in OECD TG 442E. The results for DNCB demonstrated increased expression of CD86 and CD54 after treatment, with relative fluorescence intensities (RFIs) exceeding 150% for CD86 and 200% for CD54 at concentrations ranging from 2 to 5 μg mL^{-1} and 3.5 to 5 μg mL^{-1}, respectively (Fig. S2B).

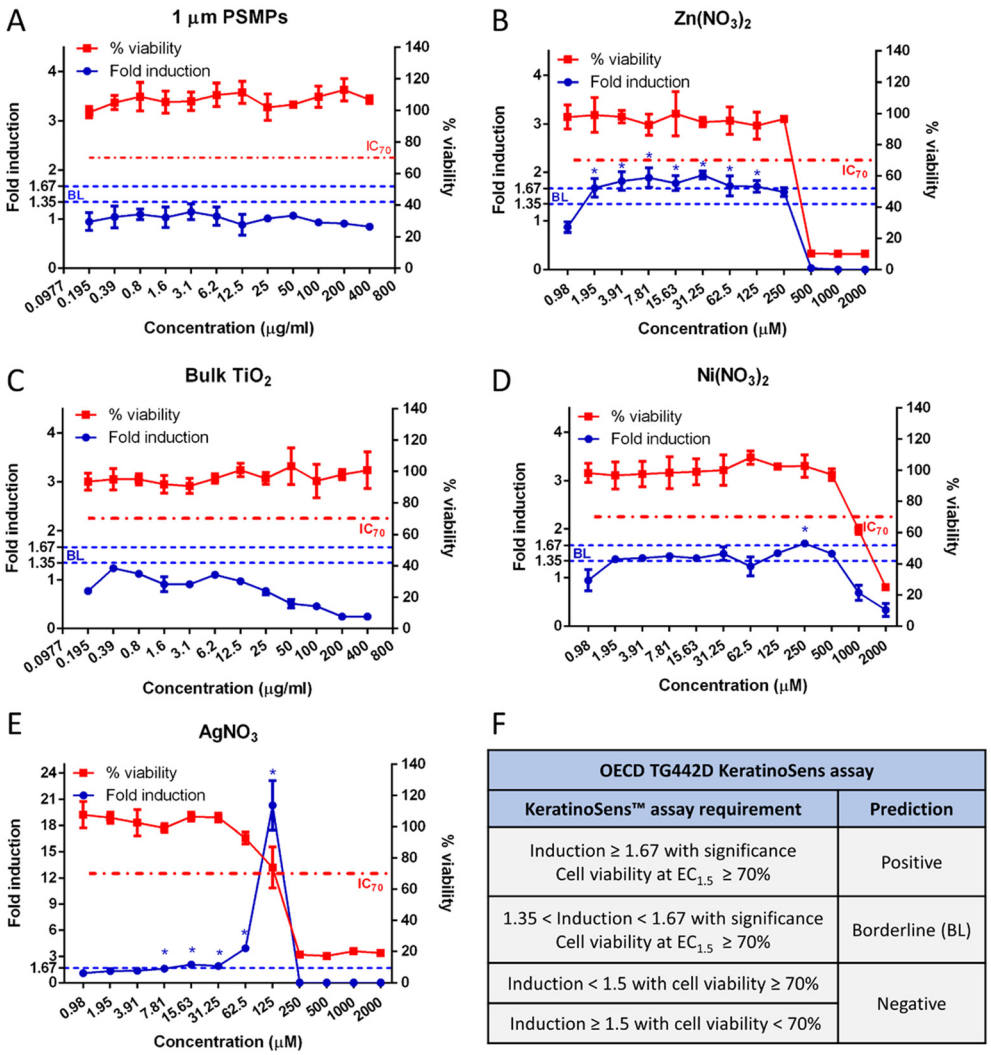

F

OECD TG442D KeratinoSens assay	
KeratinoSens™ assay requirement	Prediction
Induction ≥ 1.67 with significance Cell viability at $EC_{1.5}$ ≥ 70%	Positive
1.35 < Induction < 1.67 with significance Cell viability at $EC_{1.5}$ ≥ 70%	Borderline (BL)
Induction < 1.5 with cell viability ≥ 70%	Negative
Induction ≥ 1.5 with cell viability < 70%	

Fig. 6 KeratinoSens™ assay results of five types of corresponding materials. Dose response curve of luciferase activity induction and cell viability changes of (A) PS MPs, (B) $Zn(NO_3)_2$, (C) bulk TiO_2, (D) $Ni(NO_3)_2$, and (E) $AgNO_3$. (F) Prediction model of KeratinoSens™ assay according to OECD TG 442D. Mean ± S.D ($n \geq 3$); * p-value ≤0.05 compared to control.

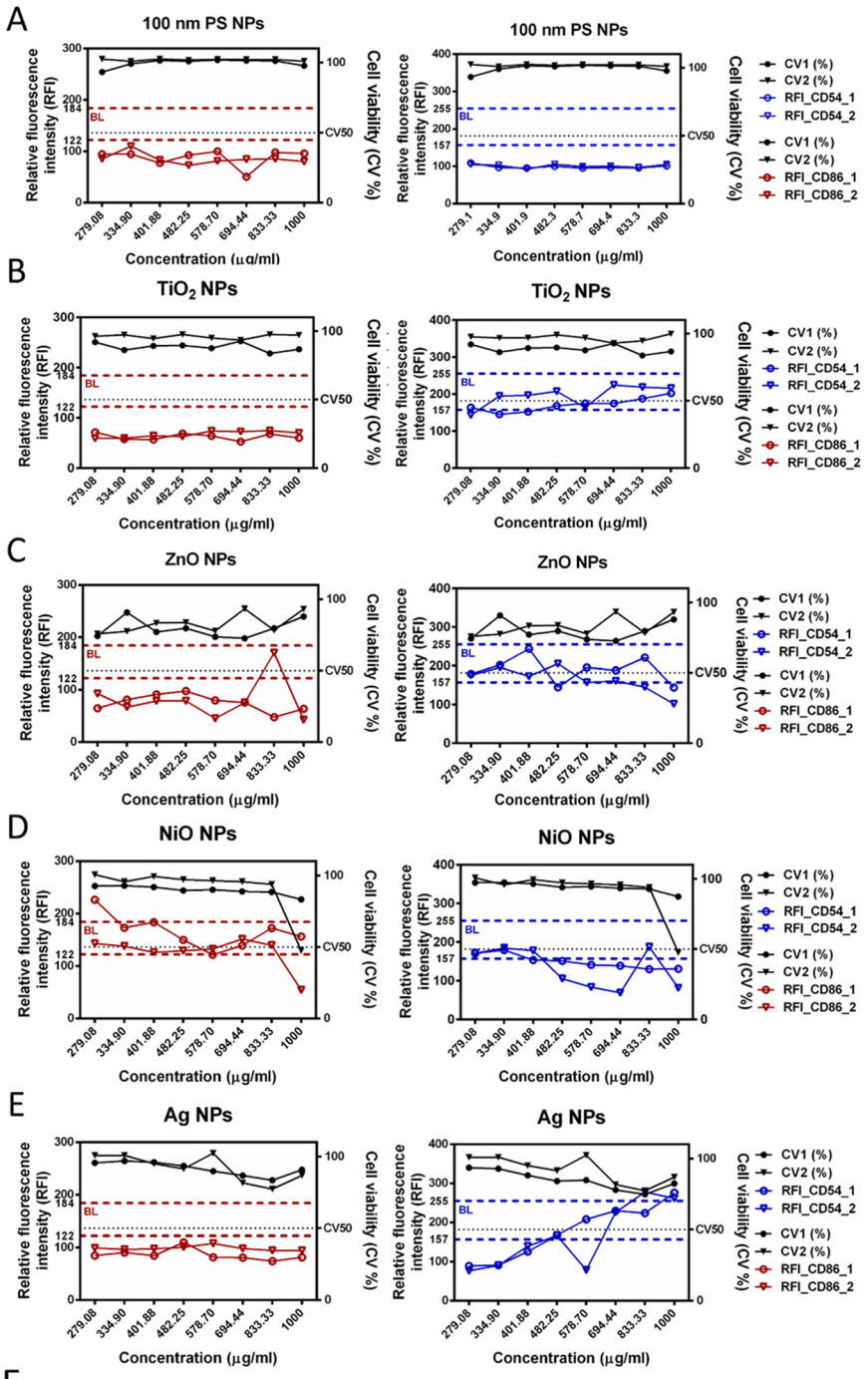

F

OECD TG442E h-CLAT assay	
h-CLAT assay requirement	**Prediction**
RFI of CD86 > 184% and/or CD54 > 255% with cell viability > 50%	Positive
122% < RFI of CD86 < 184% and/or 157% < CD54 < 255% with cell viability > 50%	Borderline (BL)
RFI of CD86 < 150% and CD54 < 200% with cell viability > 50%	Negative

Fig. 7 h-CLAT assay results of five types of nanoparticles. Dose response curve of CD86 and CD54 fluorescence induction and cell viability changes of (A) PS NPs, (B) TiO_2 NPs, (C) ZnO NPs, (D) NiO NPs, and (E) Ag NPs in serial dosage exposure. (F) Prediction model of h-CLAT assay according to OECD TG 442E. Mean ± S.D ($n \geq 3$); * p-value ≤0.05 compared to control.

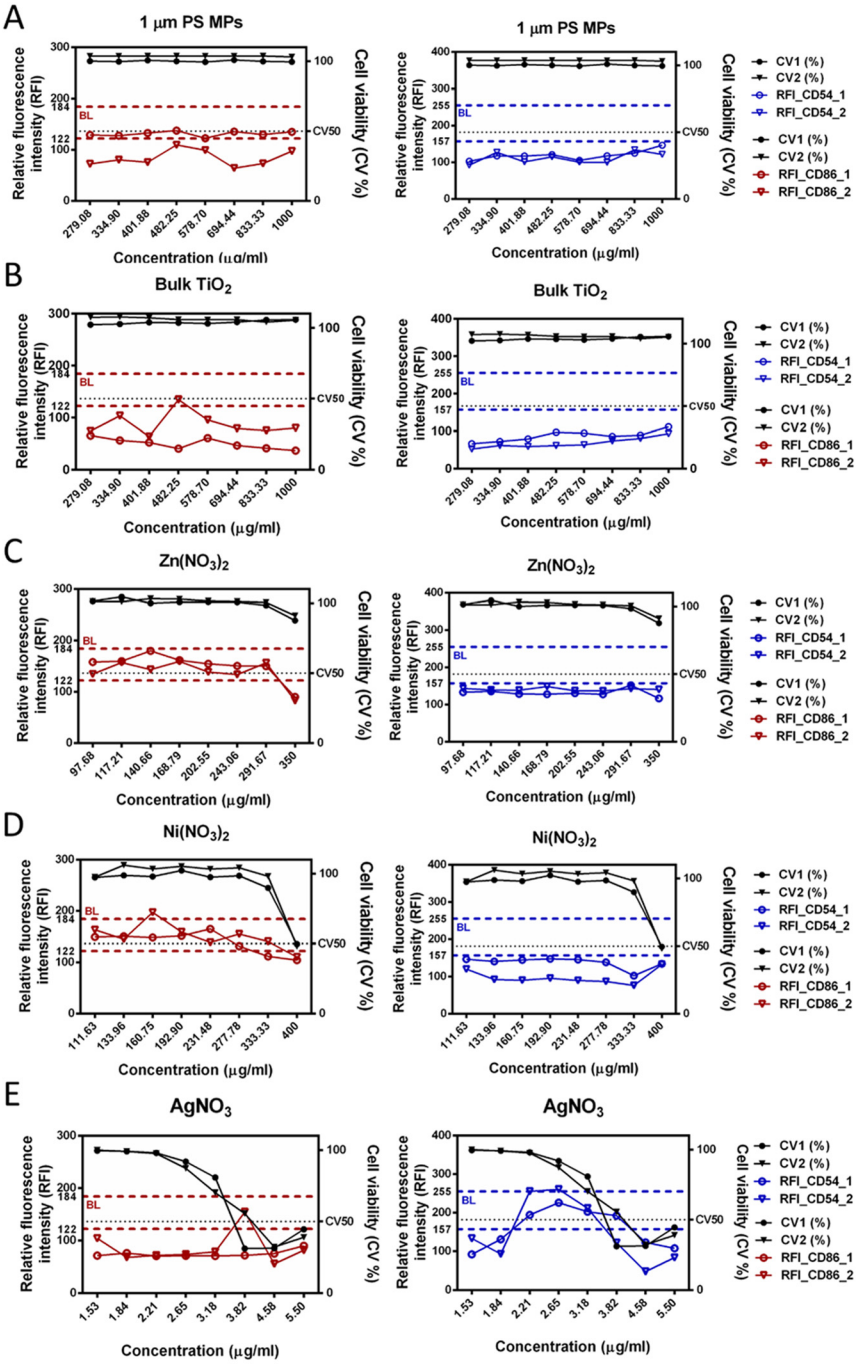

F

OECD TG442E h-CLAT assay	
h-CLAT assay requirement	**Prediction**
RFI of CD86 > 184% and/or CD54 > 255% with cell viability > 50%	Positive
122% < RFI of CD86 < 184% and/or 157% < CD54 < 255% with cell viability > 50%	Borderline (BL)
RFI of CD86 < 150% and CD54 < 200% with cell viability > 50%	Negative

Fig. 8 h-CLAT assay results of five types of corresponding materials. Dose response curve of CD86 and CD54 fluorescence induction and cell viability changes of (A) PS MPs, (B) bulk TiO_2 NPs, (C) $Zn(NO_3)_2$, (D) $Ni(NO_3)_2$, and (E) $AgNO_3$ in serial dosage exposure. (F) Prediction model of h-CLAT assay according to OECD TG 442E. Mean ± S.D ($n \geq 3$); * p-value ≤0.05 compared to control.

These results confirmed the validity of the assay and ensured the reliability of the subsequent tests.[22]

The results showed that PS NPs, PS MPs, and bulk-TiO_2 did not exceed the positive thresholds for the h-CLAT assay. Specifically, the RFI values for CD86 and CD54 remained below 150% and 200%, respectively (Fig. 7A and 8A and B). According to the prediction model in OECD TG 442E, these findings were classified as negative for skin sensitization potential (Fig. 7F and 8F). For TiO_2 NPs, no increase in the RFI of CD86 was observed, but an increase in the RFI of CD54 was detected within the range of 334.9–1000 μg mL^{-1} (Fig. 7B). ZnO NPs induced CD86 expression in one independent experiment and upregulated CD54 expression within the range of 279.08–833.33 μg mL^{-1} (Fig. 7C). Similarly, NiO NPs showed an upregulation of CD86 RFI at concentrations of 279.08–1000 μg mL^{-1}, although the increase in CD54 RFI was less pronounced (Fig. 7D). The RFIs of CD54 for TiO_2 and ZnO NPs were between 157% and 255%, while the RFI of CD86 for NiO NPs ranged from 122% to 184%. Based on the prediction model, TiO_2 NPs, ZnO NPs, and NiO NPs were classified as borderline results, requiring additional assays to confirm their sensitization potential (Fig. 7F). Ag NPs exposure in the h-CLAT assay did not alter CD86 expression but significantly induced CD54 expression within the range of 482.25–1000 μg mL^{-1}. Notably, the RFI of CD54 exceeded 255% at a concentration of 1000 μg mL^{-1} (Fig. 7E). Therefore, Ag NPs were classified as positive for skin sensitization potential (Fig. 7F).

"2o3" defined approach prediction for skin sensitization

According to the OECD Guideline No. 497 on the defined approach (DA) for classifying skin sensitization potency, the "2o3" DA was applied in this study.[23] In the 2o3 DA, test substances are classified as positive if any two test results from the OECD DPRA, KeratinoSens™, and h-CLAT assays are positive. Similarly, test substances with two concordant negative results are classified as negative. Test substances are deemed inconclusive if at least two results are borderline, or if two non-concordant results are obtained, with the third result being borderline.[23] In this study, PS NPs, PS MPs, and bulk TiO_2 were rated negative in both the KeratinoSens™ and h-CLAT assays. Consequently, the 2o3 DA conclusion for these three materials was non-sensitizer. TiO_2 NPs and ZnO NPs were classified as positive in the KeratinoSens™ assay and borderline in the h-CLAT assay. Therefore, the 2o3 DA conclusion for TiO_2 NPs and ZnO NPs was inconclusive. NiO NPs, $Zn(NO_3)_2$, $AgNO_3$, and $Ni(NO_3)_2$ were classified as borderline in both the KeratinoSens™ and h-CLAT assays, resulting in inconclusive 2o3 DA conclusions for these substances. In contrast, Ag NPs were classified as positive in both the KeratinoSens™ and h-CLAT assays. Based on the 2o3 DA, Ag NPs were concluded to be sensitizer (Table 2).

Discussion

Our study provides a comprehensive evaluation of several common industrial nanomaterials, focusing on their potential to induce skin irritation, corrosion, and sensitization using OECD-validated *in vitro* methods. The results demonstrated that while the ionic forms of metals such as silver nitrate and zinc nitrate exhibited corrosive effects, and nickel nitrate showed irritation potential, none of the NPs or bulk forms caused significant irritation or corrosion, indicating low acute dermal hazard. In contrast, sensitization testing revealed that Ag NPs showed clear sensitizing potential, while NiO NPs exhibited borderline to positive responses. TiO_2 and ZnO NPs produced inconclusive results, and PS-based materials were consistently classified as non-sensitizers. These findings underscore that although most NPs used in this study exhibited low potential for skin irritation or corrosion, certain metal-based NPs, particularly Ag and NiO, may pose sensitization risks associated with their surface reactivity and partial ion release. Importantly, the study also highlighted the need for correcting NPs-induced assay interferences to ensure reliable *in vitro* outcomes.

We began by reviewing globally available guidelines to identify key physicochemical parameters relevant to nanotoxicology. These parameters are essential for characterizing nanomaterials and understanding their behavior in different environments. According to OECD Series on the Safety of Manufactured Nanomaterials No. 36, guidance for sample preparation and characterization

Table 2 "2o3" defined approaches results of skin sensitization prediction of ten test substances

	KeratinoSens™ results				h-CLAT results				
Test substance	Imax	Viability IC 70	EC 1.5	Prediction	Viability CV 50	CD86 RFI	CD54 RFI	Prediction	Conclusion
100 nm PS NPs	1.00	>400 (μg ml^{-1})	>400 (μg ml^{-1})	Negative	>1000 (μg ml^{-1})	<150%	<200%	Negative	Non-sensitizer
1 μm PS MPs	1.08	>400 (μg ml^{-1})	>400 (μg ml^{-1})	Negative	>1000 (μg ml^{-1})	<150%	<200%	Negative	Non-sensitizer
TiO_2 NPs	1.55	1.48 (μg ml^{-1})	>400 (μg ml^{-1})	Borderline	>1000 (μg ml^{-1})	<150%	157–255%	Borderline	Inconclusive
Bulk-TiO_2	1.27	>400 (μg ml^{-1})	>400 (μg ml^{-1})	Negative	>1000 (μg ml^{-1})	<150%	<200%	Negative	Non-sensitizer
ZnO NPs	1.63	18.47 (μg ml^{-1})	39.49 (μg ml^{-1})	Borderline	>1000 (μg ml^{-1})	<150%	157–255%	Borderline	Inconclusive
$Zn(NO_3)_2$	1.95	0.35 (μM)	327.05 (μM)	Positive	<350 (μg ml^{-1})	122–184%	<200%	Borderline	Inconclusive
NiO NPs	2.15	0.381 (μg ml^{-1})	47.49 (μg ml^{-1})	Positive	<1000 (μg ml^{-1})	122–184%	<200%	Borderline	Inconclusive
$Ni(NO_3)_2$	1.70	125 (μM)	884 (μM)	Positive	<400 (μg ml^{-1})	122–184%	<200%	Borderline	Inconclusive
Ag NPs	3.38	1.671 (μg ml^{-1})	326.5 (μg ml^{-1})	Positive	<1000 (μg ml^{-1})	<150%	>255%	Positive	Sensitizer
$AgNO_3$	22.05	8.0 (μM)	223.13 (μM)	Positive	<400 (μg ml^{-1})	<150%	157–255%	Borderline	Inconclusive

primarily applies to insoluble nanomaterials, as soluble nanomaterials generally behave similarly to conventional chemicals.[51] We provided detailed physicochemical characterization of the nanomaterials used in our study, ensuring that their evaluation was thorough and aligned with established guidelines (Fig. 1). Given the diversity of nanomaterials, it remains crucial to assess these parameters on a case-by-case basis or adapt testing strategies to obtain fit-for-purpose information, as their properties can vary significantly.[52]

For skin irritation and corrosion testing, the OECD has also proposed IATA, which recommend a top-down approach for substances with substantial weight of evidence (WoE) and a bottom-up approach when evidence is lacking.[17] Based on the WoE assessments, the ionic forms of three NPs were expected to be potential skin irritants or corrosives, so we used the top-down approach for these, while the remaining others were evaluated using the bottom-up approach (Fig. 2). Previous studies commonly tested NP-induced toxicity in cell-based models at a maximum concentration of 1 mg mL^{-1}.[53–55] Following this, we applied the bottom-up method and observed that neither the NPs suspensions nor their corresponding materials (at concentrations determined by inductively coupled plasma mass spectrometry (ICP-MS)) demonstrated evidence of skin irritation or corrosion (Fig. S1). Results for the NPs and their original powder forms were consistent with their predicted irritation or corrosion potential (Fig. 2). These findings align with previous studies using OECD-validated RHE models, which also reported that these NPs do not show significant skin irritation or corrosion potential.[53,56] This may be due to the intact stratum corneum (skin) barrier in the 3D skin model,[57,58] which can limit NPs penetration and prevent further uptake.[59,60] Consistently, similar results were obtained in a previous study applying the EpiOcular™ 3D reconstructed human cornea-like epithelium (RHCE) model, where none of the tested dry-powder metal oxide NPs induced eye irritation, further supporting the low irritation potential of these materials.[61] However, the ionic forms of metal oxide NPs were identified as skin irritants or corrosives, indicating that toxicity may be driven by their released ions. This highlights the importance of considering nanomaterials solubility and ion release in toxicity assessments. Regarding the domestically developed RHE model, its validation study reported that the EPiTRI-SIT model demonstrated 100% sensitivity, 70% specificity, and 85% accuracy for skin irritation testing, meeting the performance standards of OECD TG 439.[16,49] Similarly, the EPiTRI-SCT model achieved 100% sensitivity, 80% specificity, and 93.33% accuracy for skin corrosion testing, meeting the performance standards of OECD TG 431.[15] Our study further demonstrates that the domestically developed EPiTRI model performs comparably to other validated RHE models, reinforcing its suitability for assessing both skin irritation and corrosion. Finally, our findings support the applicability of OECD TGs 439 and 431, in conjunction with GD 203, for evaluating nanomaterials-induced skin irritation/corrosion.

To evaluate the skin sensitization potential of common nanomaterials, this study used OECD-validated NAMs, which assess skin sensitization potency based on three KEs outlined in OECD guidelines: TG 442C (Direct Peptide Reactivity Assay, DPRA), TG 442D (ARE-Nrf2 Luciferase KeratinoSens™ assay), and TG 442E (human Cell Line Activation Test, h-CLAT). The DPRA was originally developed for organic compounds and has only limited validation for metal compounds.[62] Inorganic chemicals, such as transition metals and halogenated metal complexes, are generally excluded from DPRA testing because their sensitization mechanisms differ and may require an alternative AOP.[62] For example, nickel-induced skin sensitization in humans involves direct activation of toll-like receptor 4 (TLR4), triggering the production of proinflammatory mediators.[63] Substances that cannot covalently bind to peptides may yield false positive results in the DPRA due to spontaneous oxidation reactions.[64] The DPRA (OECD TG 442C) is designed to detect covalent binding of electrophilic organic chemicals to synthetic peptides containing cysteine or lysine residues. However, inorganic particles and poorly soluble metal oxides do not act through classical electrophilic haptenation mechanisms and are not expected to form stable covalent adducts with model peptides under DPRA conditions. The OECD TG 442C guideline notes limitations for substances outside the applicability domain, including materials that are insoluble, inorganic, or that interfere with spectrophotometric readouts. Therefore, conducting TG 442C would not provide biologically meaningful information for the test materials used in this study.[62–64] From a mechanistic perspective, skin sensitization is a T-cell-mediated delayed-type (type IV) hypersensitivity reaction. While KE1 (haptenation) is central for low-molecular weight organic sensitizers, non-classical sensitizers, including certain metals and particulate materials, may initiate immune activation through alternative mechanisms such as oxidative stress induction, inflammasome activation, or danger signal release. These events converge on keratinocyte activation (KE2) and dendritic cell activation (KE3), which are critical steps in the development of adaptive immune sensitization regardless of the precise molecular initiating event.[65]

NAMs for skin sensitization were originally designed for soluble chemical substances, with test endpoints based on chromogenic, fluorescence, or luciferase-based readouts. However, the potential for NPs interference in these assays remains uncertain, and current OECD guidelines do not include specific recommendations for adapting protocols for nanomaterials.[21,22] Many studies have shown that NPs can interfere with various *in vitro* assays, including viability assays, DCFH-DA assays, ELISA, and flow cytometry.[66] In the KeratinoSens™ and h-CLAT assays, cytotoxicity is assessed using the MTT assay (for KeratinoSens™) and propidium iodide (PI) staining (for h-CLAT). Our results showed that TiO_2, NiO, and Ag NPs significantly distorted the light absorption spectra of the MTT assay, resulting in inaccurate cell viability measurements and false-positive predictions in

the KeratinoSens™ assay (Fig. 4A, C and E). Similar interference with MTT and LDH assays has been reported in previous studies involving carbon black and TiO_2 NPs.[67] Other research has shown that certain NPs, including magnetic iron/graphite, magnetite/silica, PEGylated silica, and magnetite/FAU zeolite, absorb at wavelengths used in the MTT assay even in cell-free culture medium.[68] To address this, we measured the background absorbance of each NPs concentration at 570 nm and corrected the assay results. This adjustment reduced false-positive signals and improved the accuracy of the cytotoxicity measurements (Fig. 4B, D and F).

In the h-CLAT assay, CD86 and CD54 expression is measured by flow cytometry, which relies on detecting refracted laser light and fluorescence signals from cells. This technique is highly susceptible to NPs interference, which can compromise result accuracy.[66] Our findings showed that certain NPs pwere detected by the flow cytometer, generating fluorescence signals that overlapped with those of CD86 and CD54, leading to false-positive outcomes (Fig. 4I and K). Similar interference effects have been reported previously; for instance, silica NPs can induce false-positive annexin V-FITC signals by interacting with specific fluorophore combinations such as FITC/PI.[66] Conversely, some dye-based assays have shown fluorescence quenching, demonstrating that NPs can either enhance or suppress fluorescence signals depending on the assay.[66] In the h-CLAT assay, fluorescence generated by NPs can reduce the mean fluorescence intensity (MFI) of CD markers, leading to inaccurate predictions. To address this, we used DiOC18, a cell tracer dye, to distinguish cellular from NP-associated fluorescence signals. This approach allowed us to separate the cell–NPs complex and calculate CD86 and CD54 fluorescence intensity on cells alone, improving the reliability of the results. Table S1 summarizes the testing challenges and the corresponding technical modifications implemented in the KeratinoSens and h-CLAT assays.

A different pattern was observed in the *in vitro* RHE models for skin irritation and corrosion testing. According to OECD TGs 439 and 431, interference is more likely if test substances are coloured or can reduce MTT; therefore, pre-tests are recommended to assess this before running the assays. In our study, we found minimal interference from NPs in the RHE models, with levels ranging from near zero to less than 5%, indicating negligible impact on relative cell viability (Fig. S1A). This reduced interference may be due to factors such as the thorough washing steps outlined in the protocol, which effectively remove residual substances from the tissue surface and minimise prolonged contact with assay components. This prevents underestimation of relative cell viability in the MTT assay.[49] Additionally, the 3D RHE model replicates the multilayered structure of human epidermis, providing a physical barrier that limits NPs penetration. This structural feature reduces direct NP–tissue interactions during short-term exposures, minimising the risk of false assay readouts.[59,60,69] Compared to 2D skin sensitization assays, RHE models involve shorter exposure periods, further reducing the chance of NPs interfering with assay reagents or being internalised by cells.

Previous studies have investigated NAMs for assessing the skin sensitization potential of nanomaterials, but the reliability of *in vitro* assays for this purpose remains uncertain. One key aim of our study was to examine the suitability of OECD-standardized procedures for skin sensitization testing to improve prediction accuracy for NPs. The effects of PS NPs and PS MPs on human skin are not well documented, but concerns remain about their potential to cause allergic reactions due to their ability to penetrate the skin barrier.[70,71] In our study, the negative results from the KeratinoSens™ and h-CLAT assays indicated that PS NPs and PS MPs are non-sensitizers (Table 2), consistent with *in vivo* results from the Local Lymph Node Assay (LLNA).[72] Bulk TiO_2 is generally regarded as safe for use in cosmetics and produced negative results in our *in vitro* study. However, the sensitization potential of TiO_2 NPs remains debated, with conflicting findings reported. In our study, both the KeratinoSens™ and h-CLAT assays gave borderline results, resulting in an inconclusive outcome. These findings contrast with negative results observed in the LLNA and the Guinea Pig Maximisation Test (GMPT).[64,72–74] Other *in vitro* studies have also shown mixed results. For example, Bezerra *et al.* found positive results using the micro-Direct Peptide Reactivity Assay (mDPRA, OECD TG 442C) and U-SENS™ test (OECD TG 442E),[75] whereas Meindl *et al.* and Kim *et al.* reported negative results using U-SENS™ and KeratinoSens™.[76,77] Similarly, Wareing *et al.* reached an inconclusive conclusion for TiO_2 NPs using *in vitro* skin sensitization tests and DAs.[64]

The sensitization potential of metal oxide NPs also showed variability across studies. ZnO NPs were reported as non-sensitizing in patch tests and LLNA assays,[64,73] but showed inconclusive results in our study. Some studies have supported negative *in vitro* outcomes for ZnO NPs, while others have reported positive sensitization responses.[33,64,73,77,78] NiO NPs produced positive results in the KeratinoSens™ assay but borderline results in the h-CLAT assay, leading to an inconclusive prediction, although previous studies reported negative outcomes in both *in vivo* and *in vitro* tests.[73,78,79] Among the tested NPs, Ag NPs consistently produced positive results in our study and others (Table S2).[33,76] The inconsistent findings for other nanomaterials may be due to factors such as differences in NPs composition and surface properties, variations in pretreatment methods, limited interactions between cell types in *in vitro* assays, and the inability of certain NPs to penetrate the skin barrier.[64,73,77,80] Pretreatment conditions and NPs penetration were especially relevant. NPs agglomeration and dispersion states can greatly influence their physical and chemical properties, affecting sensitization responses.[73] NPs tend to agglomerate in suspension due to high surface energy and interparticle van der Waals attractions. Changes in ionic strength, pH, or the presence of

proteins in biological media can modify surface charge and lead to the formation of a protein corona, which may further promote particle aggregation and alter their biological interactions.[81] Agglomerated NPs may be blocked by the skin barrier, contributing to discrepancies between *in vivo* and *in vitro* findings.[73,80] Additionally, the degree of nanomaterials dissociation can affect sensitization potential, as seen with metal compounds in our study.[64,79] Variability may also arise from differences in how *in vitro* assays handle potential NPs interference, as correcting for interference during analysis can lead to differing outcomes. Inherent limitations of the current TGs, such as limited metabolic capacity, may still affect predictive performance. In particular, as mentioned above, NPs size and the physicochemical diversity of surface modifications may contribute to variable outcomes. Characterization of nanomaterials, as recommended in OECD TG 125 and ISO TR 22455, can provide key information, including particle size, surface area, dispersibility, and reactivity, that helps guide the choice of appropriate assays. Pre-treatment conditions, such as dispersion protocols and dosimetry, also need careful attention to ensure reliable and interpretable results. For example, TG 442C may be suitable for inorganic and non-metal nanomaterials with sufficient solubility or dispersibility, though potential assay interference still needs to be carefully evaluated. When standard *in vitro* assays cannot provide consistent conclusions, a structured, property-driven approach within the IATA framework is recommended, incorporating WoE data from additional endpoints or advanced models, such as co-culture systems or 3D skin platforms.[82,83] These approaches aim to better replicate the physiological conditions of human skin, enhancing the predictive capability of NAMs-based skin sensitization tests for nanomaterials.

Conclusions

Overall, our findings in skin irritation and corrosion assays are consistent with previous literature, demonstrating the reliability of OECD TGs 439 and 431 for assessing nanomaterials-induced skin irritation and corrosion potential. However, discrepancies were observed in skin sensitization assays, with conflicting results for certain NPs. These inconsistencies may stem from differences between 3D RHE models and two-dimensional (2D) cell culture systems, as the presence of a skin barrier in 3D models provides greater physiological relevance by limiting NPs penetration and uptake. Additionally, NPs may interfere with fluorescence-based readouts, potentially leading to inaccurate results in these *in vitro* assays. Unlike previous studies that have focused on individual NPs[33,69,76] or assessed only specific toxicity endpoints,[56,64,77,78] our study is the first to comprehensively evaluate different types of widely used NPs for their skin toxicity potential across multiple endpoints, including skin irritation, corrosion, and sensitization, as well as comparisons between these NPs and their corresponding bulk or ionic materials. By integrating IATA, DAs, and NAMs, we achieved a holistic evaluation of NPs-induced skin toxicity. However, limitations in current skin sensitization assays, such as NPs interference and predictive inconsistencies, were evident. To address these challenges, we recommend optimizing NAMs, integrating advanced 3D models, and refining calibration methods to minimize assay interference. Until these advancements are realized, animal studies may remain necessary for accurately assessing NPs-induced skin sensitization in regulatory contexts. Taken together, our study highlights the importance of combining IATA, DAs, and NAMs with traditional methods, such as animal testing data or supporting human data, to achieve a comprehensive and reliable assessment of nanomaterial-induced skin toxicity, providing valuable insights for advancing non-animal testing strategies.

Author contributions

Y-JW and R-JC contributed to the conceptualization, methodology, resources, data curation, supervision, project administration, and funding acquisition. Y-JW, OL, Y-YC, and Y-HC contributed to the original drafting of the manuscript. Y-JW, R-JC, and OL contributed to manuscript review and editing. OL, Y-YC, Y-HC, and S-NC contributed to the methodology, validation, formal analysis, investigation, data curation, and visualization. H-LC contributed to project administration. H-JC contributed to conceptualization. All authors reviewed and approved of the final manuscript.

Conflicts of interest

There are no conflicts to declare.

Data availability

The data supporting this article have been included as part of the supplementary information (SI).

The supplementary information includes supplementary figures presenting additional skin irritation/corrosion and skin sensitization test results, and supplementary tables summarizing the testing challenges, technical modifications, and available skin sensitization data for the NPs used in this study. See DOI: https://doi.org/10.1039/d5en00955c.

Acknowledgements

This work was supported by the National Science and Technology Council (NSTC 114-2314-B-006-016; NSTC 113-2314-B-006-067-MY3; NSTC 114-2622-8-006-013-TB) and Chemicals Administration, Ministry of Environment, Taiwan (No. 113DB003).

References

1 Y. Khan, H. Sadia, S. Z. Ali Shah, M. N. Khan, A. A. Shah, N. Ullah, M. F. Ullah, H. Bibi, O. T. Bafakeeh, N. B. Khedher,

S. M. Eldin, B. M. Fadhl and M. I. Khan, Classification, Synthetic, and Characterization Approaches to Nanoparticles, and Their Applications in Various Fields of Nanotechnology: A Review, *Catalysts*, 2022, **12**, 1386.

2 S. Malik, K. Muhammad and Y. Waheed, Nanotechnology: A Revolution in Modern Industry, *Molecules*, 2023, **28**, 661.

3 J. Wu, G. Gupta, T. Buerki-Thurnherr, B. Nowack and P. Wick, Bridging the Gap: Innovative Human-Based In Vitro Approaches for Nanomaterials Hazard Assessment and Their Role in Safe and Sustainable by Design, Risk Assessment, and Life Cycle Assessment, *NanoImpact*, 2024, **36**, 100533.

4 OECD, *Advanced Materials: Working Description*, OECD Publishing, Paris, 2023.

5 E. J. Petersen, P. Ceger, D. G. Allen, J. Coyle, R. Derk, N. Garcia-Reyero, J. Gordon, N. C. Kleinstreuer, J. Matheson, D. McShan, B. C. Nelson, A. K. Patri, P. Rice, L. Rojanasakul, A. Sasidharan, L. Scarano and X. Chang, U.S. Federal Agency Interests and Key Considerations for New Approach Methodologies for Nanomaterials, *ALTEX*, 2022, **39**, 183–206.

6 T. L. Srujana, K. J. Rao and T. Korumilli, Natural Biogenic Templates for Nanomaterial Synthesis: Advances, Applications, and Environmental Perspectives, *ACS Biomater. Sci. Eng.*, 2025, **11**, 1291–1316.

7 S. Schmeisser, A. Miccoli, M. von Bergen, E. Berggren, A. Braeuning, W. Busch, C. Desaintes, A. Gourmelon, R. Grafström, J. Harrill, T. Hartung, M. Herzler, G. E. N. Kass, N. Kleinstreuer, M. Leist, M. Luijten, P. Marx-Stoelting, O. Poetz, B. van Ravenzwaay, R. Roggeband, V. Rogiers, A. Roth, P. Sanders, R. S. Thomas, A. Marie Vinggaard, M. Vinken, B. van de Water, A. Luch and T. Tralau, New Approach Methodologies in Human Regulatory Toxicology – Not If, But How and When!, *Environ. Int.*, 2023, **178**, 108082.

8 F. Sewell, C. Alexander-White, S. Brescia, R. A. Currie, R. Roberts, C. Roper, C. Vickers, C. Westmoreland and I. Kimber, New Approach Methodologies (NAMs): Identifying and Overcoming Hurdles to Accelerated Adoption, *Toxicol. Res.*, 2024, **13**, tfae044.

9 B. Salieri, J. P. Kaiser, M. Rösslein, B. Nowack, R. Hischier and P. Wick, Relative Potency Factor Approach Enables the Use of In Vitro Information for Estimation of Human Effect Factors for Nanoparticle Toxicity in Life-Cycle Impact Assessment, *Nanotoxicology*, 2020, **14**, 275–286.

10 K. A. Magurany, X. Chang, R. Clewell, S. Coecke, E. Haugabrooks and S. Marty, A Pragmatic Framework for the Application of New Approach Methodologies in One Health Toxicological Risk Assessment, *Toxicol. Sci.*, 2023, **192**, 155–177.

11 D. Hristozov, E. Badetti, P. Bigini, A. Brunelli, S. Dekkers, L. Diomede, S. H. Doak, W. Fransman, A. Gajewicz-Skretna, E. Giubilato, L. Gómez-Cuadrado, R. Grafström, A. C. Gutleb, S. Halappanavar, R. Hischier, N. Hunt, A. Katsumiti, A. Kermanizadeh, A. Marcomini, E. Moschini, A. Oomen, L. Pizzol, C. Rumbo, O. Schmid, N. Shandilya, V. Stone, S. Stoycheva, T. Stoeger, B. S. Merino, L. Tran, G. Tsiliki, U. B. Vogel, W. Wohlleben and A. Zabeo, Next Generation Risk Assessment Approaches for Advanced Nanomaterials: Current Status and Future Perspectives, *NanoImpact*, 2024, **35**, 100523.

12 F. Caloni, I. De Angelis and T. Hartung, Replacement of Animal Testing by Integrated Approaches to Testing and Assessment (IATA): A Call for In Vivitrosi, *Arch. Toxicol.*, 2022, **96**, 1935–1950.

13 S. Masri, M. B. Fauzi, N. F. Rajab, W.-H. Lee, D. A. Zainal Abidin and E. L. Siew, In Vitro 3D Skin Culture and Its Sustainability in Toxicology: A Narrative Review, *Artif. Cells, Nanomed., Biotechnol.*, 2024, **52**, 476–499.

14 E. Filaire, R. Nachat-Kappes, C. Laporte, M.-F. Harmand, M. Simon and C. Poinsot, Alternative In Vitro Models Used in the Main Safety Tests of Cosmetic Products and New Challenges, *Int. J. Cosmet. Sci.*, 2022, **44**, 604–613.

15 OECD, *Test No. 431: In vitro skin corrosion: reconstructed human epidermis (RHE) test method*, OECD Publishing, Paris, 2019.

16 OECD, *Test No. 439: In Vitro Skin Irritation: Reconstructed Human Epidermis Test Method*, OECD Publishing, Paris, 2019.

17 OECD, *Guidance Document on an Integrated Approach on Testing and Assessment (IATA) for Skin Corrosion and Irritation*, OECD Publishing, Paris, 2017.

18 Y.-H. Cheng, H.-I. Wu, Y.-Y. Chen, Y.-H. Lee, B. Wang, Jr. and Y.-J. Wang, Adverse Outcome Pathway-Based Approach to Reveal the Mechanisms of Skin Sensitization and Long-Term Aging Effects of Chlorothalonil, *J. Hazard. Mater.*, 2024, **476**, 135176.

19 OECD, *The Adverse Outcome Pathway for Skin Sensitisation Initiated by Covalent Binding to Proteins*, OECD Publishing, Paris, 2014.

20 OECD, *Test No. 442C: In Chemico Skin Sensitisation: Assays Addressing the Adverse Outcome Pathway Key Event on Covalent Binding to Proteins*, OECD Publishing, Paris, 2024.

21 OECD, *Test No. 442D: In Vitro Skin Sensitisation: Assays Addressing the Adverse Outcome Pathway Key Event on Keratinocyte Activation*, OECD Publishing, Paris, 2024.

22 OECD, *Test No. 442E: In Vitro Skin Sensitisation: In Vitro Skin Sensitisation Assays Addressing the Key Event on Activation of Dendritic Cells on the Adverse Outcome Pathway for Skin Sensitisation*, OECD Publishing, Paris, 2024.

23 OECD, *Guideline No. 497: Defined Approaches on Skin Sensitisation*, OECD Publishing, Paris, 2023.

24 E. A. J. Bleeker, E. Swart, H. Braakhuis, M. L. Fernández Cruz, S. Friedrichs, I. Gosens, F. Herzberg, K. A. Jensen, F. von der Kammer, J. A. B. Kettelarij, J. M. Navas, K. Rasmussen, K. Schwirn and M. Visser, Towards Harmonisation of Testing of Nanomaterials for EU Regulatory Requirements on Chemical Safety – A Proposal for Further Actions, *Regul. Toxicol. Pharmacol.*, 2023, **139**, 105360.

25 H. Rauscher, A. Kobe, V. Kestens and K. Rasmussen, Is It A Nanomaterial in the EU? Three Essential Elements to Work It Out, *Nano Today*, 2023, **49**, 101780.

26 OECD, *Test No. 124: Determination of the Volume Specific Surface Area of Manufactured Nanomaterials*, OECD Publishing, Paris, 2022.

27 OECD, *Test No. 125: Nanomaterial Particle Size and Size Distribution of Nanomaterials*, OECD Publishing, Paris, 2023.
28 OECD, *Test No. 126: Determination of the Hydrophobicity Index of Nanomaterials Through an Affinity Measurement*, OECD Publishing, Paris, 2023.
29 J. Jeevanandam, A. Barhoum, Y. S. Chan, A. Dufresne and M. K. Danquah, Review on Nanoparticles and Nanostructured Materials: History, Sources, Toxicity and Regulations, *Beilstein J. Nanotechnol.*, 2018, **9**, 1050–1074.
30 E. J. Petersen, M. Mortimer, R. M. Burgess, R. Handy, S. Hanna, K. T. Ho, M. Johnson, S. Loureiro, H. Selck, J. J. Scott-Fordsmand, D. Spurgeon, J. Unrine, N. van den Brink, Y. Wang, J. White and P. Holden, Strategies for Robust and Accurate Experimental Approaches to Quantify Nanomaterial Bioaccumulation Across a Broad Range of Organisms, *Environ. Sci.: Nano*, 2019, **6**, 1619–1656.
31 Y.-Y. Chen, Y.-H. Lee, B.-J. Wang, R.-J. Chen and Y.-J. Wang, Skin damage induced by zinc oxide nanoparticles combined with UVB is mediated by activating cell pyroptosis via the NLRP3 inflammasome–autophagy–exosomal pathway, *Part. Fibre Toxicol.*, 2022, **19**, 2.
32 B.-J. Wang, Y.-Y. Chen, H.-H. Chang, R.-J. Chen, Y.-J. Wang and Y.-H. Lee, Zinc oxide nanoparticles exacerbate skin epithelial cell damage by upregulating pro-inflammatory cytokines and exosome secretion in M1 macrophages following UVB irradiation-induced skin injury, *Part. Fibre Toxicol.*, 2024, **21**, 9.
33 R. Gautam, S. Yang, A. Maharjan, J. Jo, M. Acharya, Y. Heo and C. Kim, Prediction of Skin Sensitization Potential of Silver and Zinc Oxide Nanoparticles Through the Human Cell Line Activation Test, *Front. Toxicol.*, 2021, **3**, 649666.
34 F. Carrouel, S. Viennot, L. Ottolenghi, C. Gaillard and D. Bourgeois, Nanoparticles as Anti-Microbial, Anti-Inflammatory, and Remineralizing Agents in Oral Care Cosmetics: A Review of the Current Situation, *Nanomaterials*, 2020, **10**, 140.
35 G. Fytianos, A. Rahdar and G. Z. Kyzas, Nanomaterials in Cosmetics: Recent Updates, *Nanomaterials*, 2020, **10**, 979.
36 W.-S. Cho, R. Duffin, F. Thielbeer, M. Bradley, I. L. Megson, W. MacNee, C. A. Poland, C. L. Tran and K. Donaldson, Zeta Potential and Solubility to Toxic Ions as Mechanisms of Lung Inflammation Caused by Metal/Metal Oxide Nanoparticles, *Toxicol. Sci.*, 2012, **126**, 469–477.
37 W.-S. Cho, B.-C. Kang, J. K. Lee, J. Jeong, J.-H. Che and S. H. Seok, Comparative Absorption, Distribution, and Excretion of Titanium Dioxide and Zinc Oxide Nanoparticles After Repeated Oral Administration, *Part. Fibre Toxicol.*, 2013, **10**, 9.
38 J. Musial, R. Krakowiak, D. T. Mlynarczyk, T. Goslinski and B. J. Stanisz, Titanium Dioxide Nanoparticles in Food and Personal Care Products-What Do We Know about Their Safety?, *Nanomaterials*, 2020, **10**, 1110.
39 A. Nawaz, A. Farhan, F. Maqbool, H. Ahmad, W. Qayyum, E. Ghazy, A. Rahdar, A. M. Díez-Pascual and S. Fathi-karkan, Zinc Oxide Nanoparticles: Pathways to Micropollutant Adsorption, Dye Removal, and Antibacterial Actions - A Study of Mechanisms, Challenges, and Future Prospects, *J. Mol. Struct.*, 2024, **1312**, 138545.
40 M. G. Berhe and Y. T. Gebreslassie, Biomedical Applications of Biosynthesized Nickel Oxide Nanoparticles, *Int. J. Nanomed.*, 2023, **18**, 4229–4251.
41 T. Bruna, F. Maldonado-Bravo, P. Jara and N. Caro, Silver Nanoparticles and Their Antibacterial Applications, *Int. J. Mol. Sci.*, 2021, **22**, 7202.
42 K. Kik, B. Bukowska and P. Sicińska, Polystyrene Nanoparticles: Sources, Occurrence in the Environment, Distribution in Tissues, Accumulation and Toxicity to Various Organisms, *Environ. Pollut.*, 2020, **262**, 114297.
43 B. Bocca, B. Battistini, V. Leso, L. Fontana, S. Caimi, M. Fedele and I. Iavicoli, Occupational Exposure to Metal Engineered Nanoparticles: A Human Biomonitoring Pilot Study Involving Italian Nanomaterial Workers, *Toxics*, 2023, **11**, 120.
44 M. Raszewska-Famielec and J. Flieger, Nanoparticles for Topical Application in the Treatment of Skin Dysfunctions-An Overview of Dermo-Cosmetic and Dermatological Products, *Int. J. Mol. Sci.*, 2022, **23**, 15980.
45 T. Piluk, G. Faccio, S. Letsiou, R. Liang and M. Freire-Gormaly, A critical review investigating the use of nanoparticles in cosmetic skin products, *Environ. Sci.: Nano*, 2024, **11**, 3674–3692.
46 F. Wang, L. Zhou, D. Mu, H. Zhang, G. Zhang, X. Huang and P. Xiong, Current research on ecotoxicity of metal-based nanoparticles: from exposure pathways, ecotoxicological effects to toxicity mechanisms, *Front. Public Health*, 2024, **12**, 1390099.
47 E. D. Tsochatzis, H. Gika, G. Theodoridis, N. Maragou, N. Thomaidis and M. Corredig, Microplastics and nanoplastics: Exposure and toxicological effects require important analysis considerations, *Heliyon*, 2024, **10**, e32261.
48 M. Viana, F. S. Tonin and C. Ladeira, Assessing the Impact of Nanoplastics in Biological Systems: Systematic Review of In Vitro Animal Studies, *J. Xenobiot.*, 2025, **15**, 75.
49 C.-C. Liao, C.-Y. Wu, M.-H. Lin, F.-K. Hsieh, L.-T. Hsu, S.-Y. Chang, K.-J. Chen, H.-T. Huang, H.-C. Hsu, C.-H. Lin, P.-J. Lin, H.-M. Lai, H. Kojima, H. Todo, S.-J. Lin, J.-H. Li and W. Chen, Validation Study of A New Reconstructed Human Epidermis Model EPiTRI for In Vitro Skin Irritation Test According to OECD Guidelines, *Toxicol. In Vitro*, 2021, **75**, 105197.
50 OECD, *Guidance Document on Good In Vitro Method Practices (GIVIMP)*, OECD Publishing, Paris, 2018.
51 OECD, *Guidance on Sample Preparation and Dosimetry for the Safety Testing of Manufactured Nanomaterials*, OECD Publishing, Paris, 2012.
52 OECD, *Physical-Chemical Parameters: Measurements and Methods Relevant for the Regulation of Nanomaterials*, OECD Publishing, Paris, 2016.
53 R. Bengalli, A. Colantuoni, I. Perelshtein, A. Gedanken, M. Collini, P. Mantecca and L. Fiandra, In Vitro Skin Toxicity of CuO and ZnO Nanoparticles: Application In the Safety Assessment of Antimicrobial Coated Textiles, *NanoImpact*, 2021, **21**, 100282.

54 J. Li, G. Diamante, I. S. Ahn, D. Wijaya, X. Wang, C. H. Chang, S.-m. Ha, K. Immadisetty, H. Meng, A. Nel, X. Yang and T. Xia, Determination of the Nanoparticle- and Cell-Specific Toxicological Mechanisms in 3D Liver Spheroids Using scRNAseq Analysis, *Nano Today*, 2022, **47**, 101652.

55 G. Gupta, F. Cappellini, L. Farcal, R. Gornati, G. Bernardini and B. Fadeel, Copper Oxide Nanoparticles Trigger Macrophage Cell Death With Misfolding of Cu/Zn Superoxide Dismutase 1 (SOD1), *Part. Fibre Toxicol.*, 2022, **19**, 33.

56 V. A. Miyani and M. F. Hughes, Assessment of the In Vitro Dermal Irritation Potential of Cerium, Silver, and Titanium Nanoparticles in a Human Skin Equivalent Model, *Cutaneous Ocul. Toxicol.*, 2017, **36**, 145–151.

57 S. Choudhury and A. Das, Advances in Generation of Three-Dimensional Skin Equivalents: Pre-Clinical Studies to Clinical Therapies, *Cytotherapy*, 2021, **23**, 1–9.

58 M. Imran, P. M. Moyle, D. Kamato and Y. Mohammed, Advances in, and Prospects of, 3D Preclinical Models for Skin Drug Discovery, *Drug Discovery Today*, 2024, **29**, 104208.

59 P. Ghasemiyeh and S. Mohammadi-Samani, Potential of Nanoparticles as Permeation Enhancers and Targeted Delivery Options for Skin: Advantages and Disadvantages, *Drug Des., Dev. Ther.*, 2020, **14**, 3271–3289.

60 N. Sadrieh, A. M. Wokovich, N. V. Gopee, J. Zheng, D. Haines, D. Parmiter, P. H. Siitonen, C. R. Cozart, A. K. Patri, S. E. McNeil, P. C. Howard, W. H. Doub and L. F. Buhse, Lack of significant dermal penetration of titanium dioxide from sunscreen formulations containing nano- and submicron-size TiO2 particles, *Toxicol. Sci.*, 2010, **115**, 156–166.

61 S. N. Kolle, U. G. Sauer, M. C. Rey Moreno, W. Teubner, W. Wohlleben and R. Landsiedel, Eye irritation testing of nanomaterials using the EpiOcular™ eye irritation test and the bovine corneal opacity and permeability assay, *Part. Fibre Toxicol.*, 2016, **13**, 18.

62 J. D. C. Hemming, M. Hosford and M. M. Shafer, Application of the Direct Peptide Reactivity Assay (DPRA) to Inorganic Compounds: A Case Study of Platinum Species, *Toxicol. Res.*, 2019, **8**, 802–814.

63 M. Carlin, M. Morant-Giner, M. Garrido, S. Sosa, A. Bianco, A. Tubaro, M. Prato and M. Pelin, Graphene-based materials are not skin sensitizers: adoption of the in chemico/in vitro OECD test guidelines, *Nanoscale*, 2025, **17**, 10932–10945.

64 B. Wareing, A. Aktalay Hippchen, S. N. Kolle, B. Birk, D. Funk-Weyer and R. Landsiedel, Limitations and modifications of skin sensitization NAMs for testing inorganic nanomaterials, *Toxics*, 2024, **12**, 616.

65 M. Aleksic, R. Rajagopal, R. de-Ávila, S. Spriggs and N. Gilmour, The skin sensitization adverse outcome pathway: exploring the role of mechanistic understanding for higher tier risk assessment, *Crit. Rev. Toxicol.*, 2024, **54**, 69–91.

66 N. Bohmer, A. Rippl, S. May, A. Walter, M. B. Heo, M. Kwak, M. Roesslein, N. W. Song, P. Wick and C. Hirsch, Interference of Engineered Nanomaterials in Flow Cytometry: A Case Study, *Colloids Surf., B*, 2018, **172**, 635–645.

67 A. Kroll, M. H. Pillukat, D. Hahn and J. Schnekenburger, Interference of Engineered Nanoparticles with In Vitro Toxicity Assays, *Arch. Toxicol.*, 2012, **86**, 1123–1136.

68 M. Awashra and P. Młynarz, The Toxicity of Nanoparticles and Their Interaction With Cells: An In Vitro Metabolomic Perspective, *Nanoscale Adv.*, 2023, **5**, 2674–2723.

69 L. Chen, M. Wu, S. Jiang, Y. Zhang, R. Li, Y. Lu, L. Liu, G. Wu, Y. Liu, L. Xie and L. Xu, Skin Toxicity Assessment of Silver Nanoparticles in a 3D Epidermal Model Compared to 2D Keratinocytes, *Int. J. Nanomed.*, 2019, **14**, 9707–9719.

70 E. Winiarska, M. Jutel and M. Zemelka-Wiacek, The Potential Impact of Nano-and Microplastics on Human Health: Understanding Human Health Risks, *Environ. Res.*, 2024, **251**, 118535.

71 A. Menichetti, D. Mordini and M. Montalti, Penetration of Microplastics and Nanoparticles Through Skin: Effects of Size, Shape, and Surface Chemistry, *J. Xenobiot.*, 2024, **15**, 6.

72 Y.-H. Park, S. H. Jeong, S. M. Yi, B. H. Choi, Y.-R. Kim, I.-K. Kim, M.-K. Kim and S. W. Son, Analysis for the Potential of Polystyrene and TiO2 Nanoparticles to Induce Skin Irritation, Phototoxicity, and Sensitization, *Toxicol. In Vitro*, 2011, **25**, 1863–1869.

73 D. H. Lee, S.-H. Kim, J. H. Lee, J.-Y. Yang, J.-H. Seok, K. Jung and J. K. Lee, Flow Cytometric Evaluation of The Potential of Metal Oxide Nanoparticles for Skin Sensitization Using 5-Bromo-2-Deoxyuridine, *Toxicol. Res.*, 2021, **37**, 369–377.

74 S. Smulders, L. Golanski, E. Smolders, J. Vanoirbeek and P. Hoet, Nano-TiO2 Modulates the Dermal Sensitization Potency of Dinitrochlorobenzene After Topical Exposure, *Br. J. Dermatol.*, 2015, **172**, 392–399.

75 S. F. Bezerra, B. dos Santos Rodrigues, A. C. da Silva, R. I. de Avila, H. R. Brito, E. R. Cintra, D. F. Veloso, E. M. Lima and M. C. Valadares, Application of the Adverse Outcome Pathway Framework for Investigating Skin Sensitization Potential of Nanomaterials Using New Approach Methods, *Contact Dermatitis*, 2021, **84**, 67–74.

76 J. S. Kim, K. S. Song, J. H. Sung, H. R. Ryu, B. G. Choi, H. S. Cho, J. K. Lee and I. J. Yu, Genotoxicity, Acute Oral and Dermal Toxicity, Eye and Dermal Irritation and Corrosion and Skin Sensitisation Evaluation of Silver Nanoparticles, *Nanotoxicology*, 2013, **7**, 953–960.

77 C. Meindl, K. Öhlinger, V. Zrim, J. Ober, R. Jeitler, E. Roblegg and E. Fröhlich, Skin Sensitization Potential of Sensitizers in the Presence of Metal Oxide Nanoparticles In Vitro, *Nanomaterials*, 2024, **14**, 1811.

78 S.-H. Kim, D. Lee, J. Lee, J.-Y. Yang, J. Seok, K. Jung and J. Lee, Evaluation of the Skin Sensitization Potential of Metal Oxide Nanoparticles Using the ARE-Nrf2 Luciferase KeratinoSens TM Assay, *Toxicol. Res.*, 2021, **37**, 277–284.

79 S.-H. Kim, J. H. Lee, K. Jung, J.-Y. Yang, H.-S. Shin, J. P. Lee, J. Jeong, J.-H. Oh and J. K. Lee, Copper and Cobalt Ions

Released from Metal Oxide Nanoparticles Trigger Skin Sensitization, *Front. Pharmacol.*, 2021, **12**, 627781.

80 B. Dréno, A. Alexis, B. Chuberre and M. Marinovich, Safety of Titanium Dioxide Nanoparticles in Cosmetics, *J. Eur. Acad. Dermatol. Venereol.*, 2019, **33**, 34–46.

81 M. Gorohovs and Y. Dekhtyar, Surface Functionalization of Nanoparticles for Enhanced Electrostatic Adsorption of Biomolecules, *Molecules*, 2025, **30**, 3206.

82 D. Gądarowska, J. Kalka, A. Daniel-Wójcik and I. Mrzyk, Alternative Methods for Skin-Sensitization Assessment, *Toxics*, 2022, **10**, 740.

83 M. T. Schellenberger, U. Bock, J. Hennen, F. Groeber-Becker, H. Walles and B. Blömeke, A Coculture System Composed of THP-1 cells and 3D Reconstructed Human Epidermis to Assess Activation of Dendritic Cells by Sensitizing Chemicals After Topical Exposure, *Toxicol. In Vitro*, 2019, **57**, 62–66.

